universität wien

MASTERARBEIT / MASTER'S THESIS

Titel der Masterarbeit / Title of the Master's Thesis

New insights into the biochemistry and target specificity of the ADP-ribosylating exotoxins *Aeromonas salmonicida* AexT and *Pseudomonas aeruginosa* ExoT

verfasst von / submitted by

Carmen Ebenwaldner, BSc

angestrebter akademischer Grad / in partial fulfilment of the requirements for the degree of

Master of Science (MSc)

Wien, 2022 / Vienna, 2022

Studienkennzahl lt. Studienblatt / degree programme code as it appears on the student record sheet:	UA 066 834
Studienrichtung lt. Studienblatt / degree programme as it appears on the student record sheet:	Molekulare Biologie / Molecular Biology
Betreut von / Supervisor:	Dr. Dea Slade, PhD

Table of Contents

SUMMARY

ADP-ribosylation is a post-translational modification exploited by many pathogens to facilitate the pathogen's entry into host cells, spread, and evasion from the host immune system. One common mechanism is the disruption of the cytoskeleton, either via modification of factors in upstream signaling pathways or by the direct modulation of structural components.

Pseudomonas aeruginosa exotoxins T and S (ExoT, ExoS) and *Aeromonas salmonicida* ADP-ribosyltransferase toxin (AexT) are able to ADP-ribosylate components of these groups of proteins. Despite their high level of conservation, their target spectra differ.

Bioinformatic analyses revealed that the regions conferring target specificity in the *Pseudomonas* exotoxins are highly conserved between AexT and ExoT, but are different in ExoS. This observation prompted us to investigate the target spectrum of AexT and ExoT and compare them biochemically. The aggregation-prone recombinant toxins were recovered from *E.coli* inclusion bodies. Through protein overlay assays I found that both toxins possess auto-modification activity, resulting in higher processing rates in enzymatic assays compared to the more soluble isolated catalytic domains. I could show that both toxins modify actin and CRK proteins *in vitro*, which are known targets for AexT and ExoT respectively. Furthermore, my results suggest that the toxins' ADP-ribosylation activity is specific for arginines. Although the modification of actin impairs actin polymerization *in vitro*, I found that the canonical arginine 177 might not be the only residue that is modified within actin. Our analyses highlight the dimensions of the arsenal of the toxins that enable host infection by *P.aeruginosa* and *A.salmonicida*.

ZUSAMMENFASSUNG

ADP-Ribosylierung ist eine posttranslationale Modifikation, die von vielen pathogenen Bakterien genutzt wird, um das Eindringen in Wirtszellen sowie die Ausbreitung des Erregers zu erleichtern und dem Immunsystem des Wirts zu entkommen. Ein gängiger Mechanismus ist die Störung des Zytoskeletts, entweder durch die Modifikation von Signalfaktoren oder durch die direkte Modulation von Strukturkomponenten.

Die Exotoxine T und S (ExoT, ExoS) von *Pseudomonas aeruginosa* und das homologe Toxin (AexT) von *Aeromonas salmonicida* sind in der Lage, Komponenten dieser Gruppen von Proteinen zu ADP-ribosylieren. Trotz ihrer hohen Konservierung haben sie unterschiedliche Zielspektra.

Bioinformatische Analysen ergaben, dass die Regionen, die den *Pseudomonas*-Exotoxinen ihre Substratspezifität verleihen, zwischen AexT und ExoT stark konserviert sind, während sie sich bei ExoS unterscheiden. Diese Beobachtung veranlasste uns, AexT und ExoT in Hinblick auf ihre Zielspektra und ihre Biochemie erneut zu untersuchen. Da die rekombinanten Toxine leicht aggregieren, wurden sie aus *E.coli*-Einschlusskörpern gewonnen. Mit Hilfe von Protein-Overlay-Assays fand ich heraus, dass sich beide Toxine selbst modifizieren, was dazu führt, dass sie in enzymatischen Assays im Vergleich zu den besser löslichen katalytischen Domänen höhere Prozessraten aufweisen. Ich konnte zeigen, dass beide Toxine Aktin und CRK-Proteine *in vitro* modifizieren, die jeweils als spezifisch für die Modifikation durch AexT bzw. ExoT galten. Meine Resultate weisen darauf hin, dass die ADP-Ribosylierungsaktivität der Toxine spezifisch für Arginine ist. Obwohl die Modifikation von Aktin die Aktin-Polymerisation *in vitro* beeinträchtigt, ist das kanonische Arginin 177 möglicherweise nicht der einzige Aminosäurerest, der in Aktin modifiziert wird. Unsere Analysen verdeutlichen die Dimensionen des Arsenals der Toxine, die eine Infektion des Wirts durch *P.aeruginosa* und *A.salmonicida* erleichtern.

ACKNOWLEDGMENTS

I would like to thank the Protein Science Facility, Karolinska Institutet, Stockholm for molecular cloning of parental vectors as well as the Lund Protein Production Platform for SEC-MALS (OMISEC) analysis. Thanks should also go to Dr. Ivan Ahel for providing the ARH1 expression vector, to Dr. Archimede Torretta for his help with structural modeling and model representation in Chimera, and Tommy Dam for providing Jurkat cells. Special thanks go to Dr. Antonio Ginés García Saura for help with structural modeling, and providing purified ADP-ribosylhydrolases, CRK and CRKL constructs, eAF1521-GFP, C2I and PARP10.

I would also like to express my gratitude for the generous financial support by the National Agency Erasmus+ Austria as well as the association Wirtschaft für Bildung of the Industriellenvereinigung Kärnten.

Many thanks need to go to Dr. Dea Slade for shaping my career path by opening a window to protein biochemistry and research in post-translational modifications. She readily agreed to take on the role of official supervisor at the University of Vienna and would support me wherever she could. I am grateful to have had the opportunity to work with her and I am looking forward to our encounters at international conferences in the field of ADP-ribosylation.

I could not have undertaken this journey without the help of my on-site supervisor Dr. Herwig Schüler who was never deterred by any bureaucratic barriers or organizational difficulties. Thank you for treating me as an equal, always listening to my ideas and encouraging me in my projects. I am already looking forward to many new challenges in and with your laboratory. Words cannot express my gratitude for Antonio, who has supported me without assuming compensation since the day I arrived. I got to know him as the sharp-witted and committed scientist that he is. He helped me forming hypotheses, taught me to think critically and would always be grateful to listen to my opinion in the rare occasions in which he was stuck. Since Mathieu and Archimede came to our lab, working days are much livelier. I love our fruitful scientific discussions, always accompanied by a spark of Mediterranean spirit.

Lastly, I would like to thank my friends and family for their genuine support, specifically my parents and my aunt Anni. When you are proud, I am happy.

This thesis is dedicated to the memory of my uncle Herwig Spieß.

INTRODUCTION

ADP-ribosylation is a post-translational modification that is thought to have evolved in bacteria as an anti-viral defense mechanism. From there, it expanded to all kingdoms and evolved to have multiple roles in the maintenance of normal cell function but also in pathogenesis.[1,2] The attachment of an ADP-ribose moiety onto target molecules is catalyzed by enzymes of the ART (ADP-ribosyltransferase) superfamily and involves the hydrolysis of a nicotinamide adenine dinucleotide (NAD^+) molecule and subsequent formation of an N-, O-, or S-glycosidic bond. The cumbersome ADP-ribose moiety can be attached to proteins, DNA, RNA, and even small molecules as a single unit or as long and branched polymers, depending on the enzyme.[1–3] ADP-ribosylation has wide-ranging effects such as promoting or inhibiting intermolecular interactions, modifying enzymatic activity, or regulating the stability of the modified substrate, to name a few.[2] All ARTs share a conserved core structure, called the ART fold, which comprises a split β-sheet that forms the highly specific binding site for NAD^+. The co-substrate is held in place in a bent conformation that facilitates the hydrolysis of the glycosidic bond by lowering the activation energy.[1,2] The ARTs can be subdivided into two groups, depending on the residues in the catalytic triad that perform NAD^+ hydrolysis and attachment of ADP-ribose. The HYE ARTs contain a histidine-tyrosine-glutamate motif and form the diphtheria toxin family, named after the first organism, *Corynebacterium diphtheria*, in which they were identified. The RSE ARTs were first described in *Vibrio cholerae*, therefore called the cholera toxin family, and possess an arginine, a serine, and a glutamate residue in the active site.[1–3]

Although originally evolved as a defense mechanism, many bacteria adapted to deploy ADP-ribosylating enzymes for their own infection strategies. Needless to mention, *C.diphtheria* and *V.cholerae* in which the first ARTs were identified, are two well-known examples. The molecular mechanism of the cytotoxicity of those pathogens is as complex as the pathological consequences that enable dissemination, evasion of the immune system, and damage to the host.[4,5] ADP-ribosylation of EF2 (elongation factor 2) by exotoxin A of *Pseudomonas aeruginosa* for example leads to the discontinuation of all protein production within the infected cell, with dramatic consequences eventually leading to apoptosis.[6] Cholera toxin on the other hand ADP-ribosylates the heterotrimeric G protein G_s at the Gα subunit, leading to an increase in cAMP production which in turn results in the secretion of ions and water into the intestinal lumen, leading to dysentery.[5] Many toxins direct their ADP-ribosylating activities towards factors involved in the regulation of the host cytoskeleton. On the one hand, the inactivation of factors in the Rho GTPase signaling cascades that regulate the cytoskeleton results in morphological changes that prevent bacterial uptake by macrophages and leads to the weakening of the epithelial barrier function which promotes colonization. On the other hand, some toxins specialized to directly ADP-ribosylate actin on one single residue, arginine 177 (R177), positioned at the interface of adjacent

monomers in the actin filament, leading to the depolymerization of actin. The infected cell undergoes morphological changes that impede the normal immune response.[5,7,8]

Exotoxin T (ExoT) of *Pseudomonas aeruginosa* employs the indirect pathway by blocking Rac-mediated phagocytosis through ADP-ribosylation of upstream CRK adaptor proteins.[9] Apart from ExoT, *P.aeruginosa* has many other virulence factors including adhesins, proteases, phospholipases, and other exotoxins.[6] Exotoxins U, S, T, and Y are directly injected via the type-three secretion system into the host cell cytoplasm[6], whereas Exotoxin A uptake is regulated by receptor-mediated endocytosis.[4] Only ExoS, ExoT, and ExoA possess ADP-ribosylating activities whereas ExoU is a phospholipase and ExoY has adenylate cyclase activity.[6,10] Due to the multitude of virulence factors in combination with the fast adaptation to environmental factors, including antibiotics, *P.aeruginosa* infections are difficult to treat and have a high morbidity and mortality rate. Most infections are nosocomial, i.e. acquired in the hospital, and mainly affect immunocompromised individuals such as fire victims or cystic fibrosis patients.[6]

AexT of *Aeromonas salmonicida* ADP-ribosylates actin at R177, thereby directly inhibiting actin polymerization in the infected cell.[11] Other prominent members of that group are C2 toxin of *Clostridium botulinum* and Iota toxin of *Clostridium perfringens*.[7] Apart from AexT, other virulence factors have been found in *Aeromonas* species, of which the most cytotoxic ones are directly injected into host cells via the type three secretion system. Out of all identified enzymes that are delivered during infection, more than half have been shown to alter the regulation of the host cell cytoskeleton. AexT however seems to be the only ADP-ribosylating enzyme among all injected virulence factors.[12] As ExoT, AexT belongs to the cholera toxin family of ARTs, by virtue of the RSE motif in the catalytic site.[5] Acute infection of the host, i.e. salmonids for the most part, eventually causes furunculosis, a disease that is still causing huge economic losses in salmonid aquacultures.[13,14]

Both infections with ExoT and AexT were demonstrated to induce a cell rounding phenotype in cultured cell lines, which was only partially attributed to their ADP-ribosylating activity.[11,15] In fact, both toxins are bifunctional enzymes and share a very similar domain structure. Whereas the C-terminal part contains the ART domain, the N-terminus comprises a GTPase activating protein (GAP) domain.[11,16] Upon entry into the cell, the toxins' ADP-ribosyltransferase activities are activated through tight binding to host-derived 14-3-3 proteins.[17,18] The highly conserved eukaryotic 14-3-3 proteins promote protein-protein interactions through the formation of homo- and heterodimers. Hundreds of different interaction partners have been identified so far, making the proteins indispensable in various processes, ranging from signal transduction, folding assistance, and protein localization to cell-cycle control and apoptosis.[19] ExoS was shown to

interact with all seven mammalian 14-3-3 isoforms, with the tightest interaction formed with 14-3-3β.[18]

ExoT was first described to act as a GTPase activating protein against Rho, Rac, and Cdc42 *in vitro*[20] and later *in vivo*.[21] Around the same time, the GAP activity of ExoT was discovered to be accountable for changes in cell morphology of infected cells, such as disassembly of stress fibers, cell rounding, and anti-internalization effects.[15,21] The residual effects on the morphology of cells infected with a GAP-activity deficient mutant of ExoT suggested that other regions outside of the GAP domain also play a role in the disruption of the cytoskeleton.[15] Shortly after, it was discovered that the ADP-ribosylating activity of ExoT accounts for the observed residual phenotype and that only inactivation of the activities of both catalytic domains by point mutations would abrogate all effects on infected cells.[9,22] AexT was first described by Braun et al. to be an ADP-ribosylating enzyme that causes cell rounding of infected cultured fish cells.[23] Later on, AexT was shown to also possess GAP activity towards Rho, Rac, and Cdc42 and it was demonstrated that both enzymatic domains need to be functional in order to cause the full cell rounding effect in infected cells.[11]

The manipulation of Rho GTPases is a common mechanism of bacterial toxins to enable infection, colonization, and proliferation within the host. Depending on the pathogen's needs, the target protein function is activated or inactivated with opposing effects on the host cytoskeleton. Pathogens that proliferate within the host cells to evade the immune system activate host Rho GTPases, thereby triggering actin polymerization, the formation of stress fibers, and focal point formation which eventually leads to pathogen internalization by the cells. On the contrary, the invasion strategy of some pathogens includes impairment of epithelial and endothelial barrier functions to promote dissemination and the prevention of phagocytosis by macrophages. This is achieved by toxins that inactivate Rho GTPases, leading to actin depolymerization, cell rounding, and loss of tight and adherence junctions as well as actin stress fibers. *P.aeruginosa* and *A.salmonicida* belong to the latter group of pathogens. ExoT and AexT inactivate Rho, Rac, and Cdc42 of the Rho GTPase family by mimicking eukaryotic GAP proteins.[8] ExoS, the second RSE type ART expressed in *Pseudomonas*, is a homolog of ExoT and AexT, with a highly similar domain structure. Its GAP domain was shown to inactivate the same Rho family GTPases, but its ART-targets differ from both ExoT and AexT.[16]

Despite the high conservation of ExoS, ExoT, and AexT ART domains, it is intriguing that the toxins are so different in their ADP-ribosylation target substrate specificity. Sun and co-workers discovered six low-homology regions between ExoS and ExoT, whereupon they hypothesized that those regions define the differences in target recognition between the two otherwise so similar exotoxins. Through the construction of multiple ExoT and ExoS mutants, the authors identified

regions B, C, and E to be necessary and sufficient for ExoS target recognition. Those regions reside within well-defined motifs of the ART fold. Region B and region C constitute the core of the active site loop and the ARTT (ADP-ribosylating toxin turn-turn) motif, respectively, which have both previously been suggested to play a role in substrate recognition.[24,25] Region E comprises only two residues in ExoT[26] and lies within a motif referred to as the PN (phosphate nicotinamide) loop in *Clostridium botulinum* C3 toxin which is involved in the stabilization of the NAD^+ molecule.[27] In addition to those three regions, region A (helix α1) was shown to be necessary for ExoT ADP-ribosylation specificity.[26]

Sequence alignment of AexT with the two *P.aeruginosa* exotoxins and structural analysis of an $AexT_{ART}$ model suggest a good conservation with ExoT - but not with ExoS - in the regions necessary for substrate recognition. This observation prompted us to re-analyze the target spectrum of ExoT and AexT and compare their biochemical characteristics. Due to their high intrinsic aggregation propensity, the full-length toxins are challenging to purify. In the course of this project, I optimized a purification protocol with which I accomplished to recover the full-length toxins from *E.coli* inclusion bodies. Biochemical comparison with their easier to purify ART domains highlighted the extensive auto-modification activity of the full-length variants. With the help of protein overlay assays, I could show that the ExoT and AexT ADP-ribosylating activities are indeed directed towards the same protein targets. Although I could show that ExoT and AexT ADP-ribosylation activities are arginine-specific, my results indicate that R177 is not the only residue that is being modified in actin. Independent of the nature of the modification, AexT and ExoT ADP-ribosylation of actin impairs actin polymerization *in vitro*. Our data highlights the similarity of AexT and ExoT and indicates that both toxins have a multitude of possibilities to affect the integrity of the host cytoskeleton.

RESULTS

Aeromonas salmonicida AexT is closely related to *Pseudomonas aeruginosa* ExoT

To investigate the similarity between the three homologous exotoxins AexT, ExoT, and ExoS, we compared them computationally on the sequence and structural level. The amino acid sequences of the exotoxins AexT, ExoT, and ExoS were aligned with the ClustalO algorithm **(Appendix Fig. 1)**. ExoT and ExoS, both from *Pseudomonas aeruginosa*, are the most conserved pair among the three, with a sequence identity of 74,4%. In contrast, *Aeromonas salmonicida* AexT shares 54,38% and 59,01% sequence homology with ExoS and ExoT, respectively. **Figure 1A** shows the alignment of the C-terminal sequences, comprising two LDLA-boxes that have been shown to bind in the 14-3-3β phosphoprotein binding site in the case of $ExoS_{ART}$ and $ExoT_{ART}$.[18] The similarity on the amino acid level is also depicted in the target spectrum of the toxins. The GAP domains of all three exotoxins target the GTPases Rho, Rac, and Cdc42,[11,16] although the sequence conservation between AexT and the *Pseudomonas* toxins is less pronounced in this region of the proteins (**Fig. 1B**). On the contrary, the ART domain is highly conserved among all three toxins, but the specificity differs. ExoS has been described as a polysubstrate-specific enzyme, targeting among other proteins Rho, Rac, K-Ras, and vimentin, and undergoes auto-modification. ExoT was found to ADP-ribosylate PGK-1, CRK-I, and CRK-II, and also modifies itself.[9,16] AexT on the other hand appears to be exclusively modifying actin.[11]

Crystal structures of $ExoT_{ART}$ and $ExoS_{ART}$ in complex with their chaperone 14-3-3β have been solved. The authors showed that the ART domains exist in different complexes in solution, among which heterotetramers and heterotrimers were the most prominent forms that also crystallized.[18] No structure of AexT is available in the RCSB protein data bank. Based on the closer homology to $ExoT_{ART}$, we decided to use the existing $ExoT_{ART}$ crystal structure as a template to build an $AexT_{ART}$ homology model in SWISS-MODEL.[28] We aligned the model with the existing $ExoT_{ART}$:14-3-3β structure in Chimera and deleted the $ExoT_{ART}$ molecules, to show $AexT_{ART}$ on top of the 14-3-3β homodimer (**Fig. 1C and Appendix Fig. 2A**). Although the 14-3-3β molecules were not included in modeling, LDLA box-1 of the $AexT_{ART}$ model fits very well into the phosphoprotein binding site of 14-3-3β (**Appendix Fig. 2B**). Depiction of the electrostatic surface potential of the $AexT_{ART}$ model shows the hydrophobic surfaces that are presumably involved in 14-3-3β binding (**Fig. 1D, E**), as has been shown for $ExoT_{ART}$ and $ExoS_{ART}$.[18]

To illustrate the active site, we placed a carba-NAD molecule into the NAD^+ binding site (**Fig. 1C and Appendix Fig. 2B**), according to an existing $ExoS_{ART}$:14-3-3β structure.[18] AexT belongs to the RSE ART superfamily, indicating that an arginine, a serine, and a glutamate residue form the catalytic triad. The conserved arginine fulfils the role of correctly positioning the NAD^+ molecule in the active site through the formation of electrostatic interaction with the diphosphates. The glutamate at the third position of the RSE motif is part of an EXE motif (where X could be any

amino acid). One of the two glutamates promotes the transfer of the ADP-ribose onto an acceptor residue, and the other glutamate arranges the NAD^+ molecule in a manner that facilitates hydrolysis.[2,5] However, AexT deviates from the canonical positioning of the catalytic glutamates within the primary sequence compared to other RSE ARTs. According to the sequence alignment with ExoT and ExoS the catalytic glutamates would be represented by E401 and E403 in AexT. However, E403 has been shown to be dispensable for catalytic activity in AexT. Instead, E398 takes over the role, resulting in an EXXE motif[11] **(Appendix Fig. 1)**. A close-up view of the active site in our $AexT_{ART}$ model, with the inhibitor STO1101 that was included in modeling, illustrates the active site residues as well as two other arginines R306 and R340 that are within 5 Å distance of the ligand. Although the identity of the catalytic glutamates has been confirmed by the construction of double and triple mutants in AexT[11], it is remarkable that the more distant E398 takes over the function of E403 (**Appendix Fig. 2C**). However, as E398 sits on a small alpha-helical segment that is flanked by loops, this might be explained by a high flexibility of the residue. The same study showed that R303 represents the catalytic residue essential for AexT activity.[11] Again, based on our $AexT_{ART}$ model, R306 and R340 seem to be more plausible candidates to adopt that function.

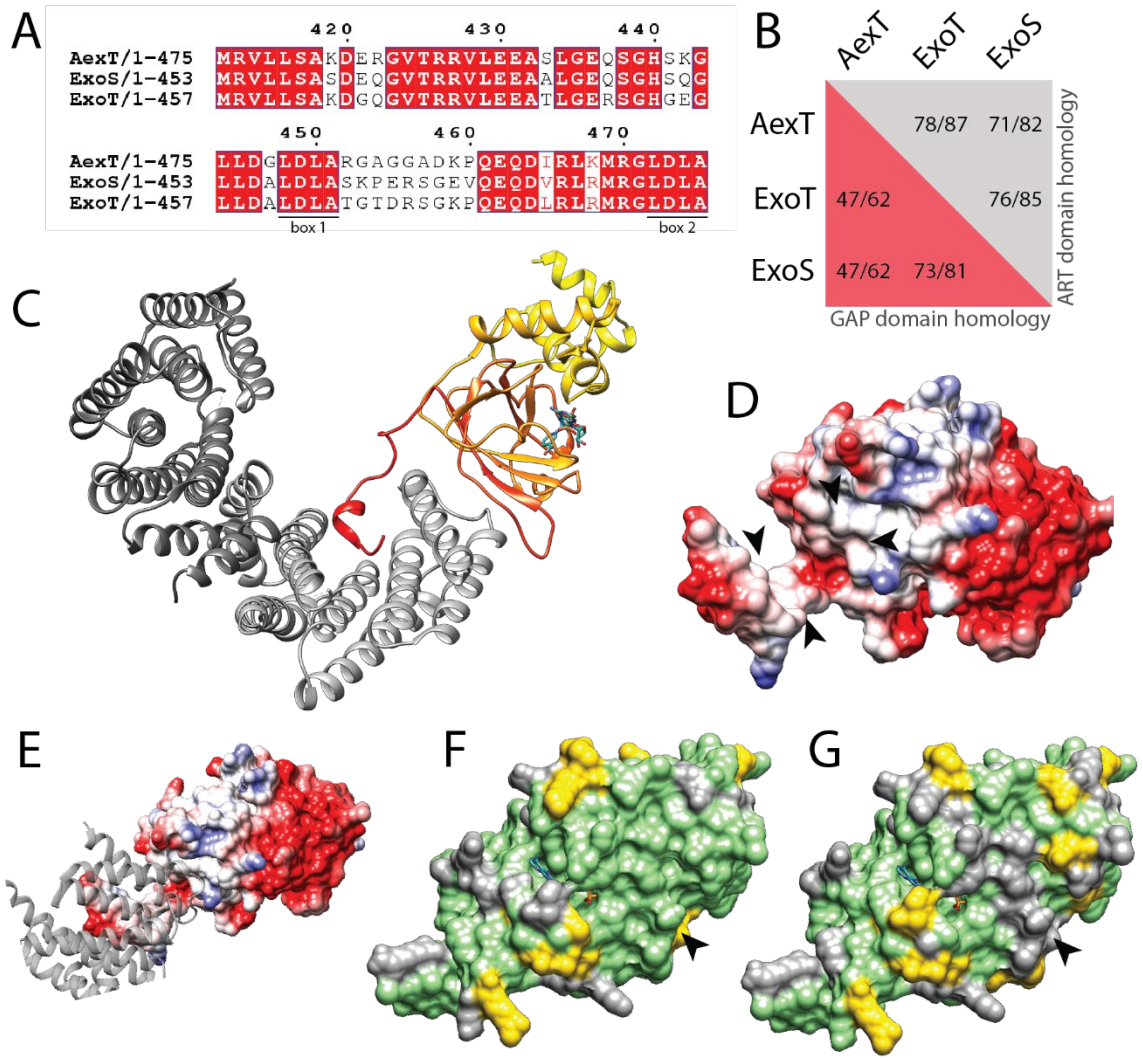

Figure 1 Homology relations of *Aeromonas* AexT with *Pseudomonas* ExoT and ExoS. **(A)** Sequence alignment of the C-termini of the three exotoxins, containing two LDLA boxes involved in 14-3-3 binding.[18] **(B)** Sequence homologies of the GAP and ART domains of the three exotoxins. Especially the ART domains are highly conserved. Homologies are given in the format %identity/%similarity. **(C)** AexT homology model based on the ExoT crystal structure 6gnn, placed on the 14-3-3β homodimer.[18] The color gradient indicates the directionality from N- (yellow) to C-terminus (red). A carba-NAD molecule was illustratively placed in the active side. **(D, E)** Surface representation of the AexT homology model, indicating the electrostatic potential (red, acidic; blue, basic; white, apolar) with emphasis on the 14-3-3 binding site, either marked with arrowheads **(D)** or indicated by the 14-3-3β crystal structure in grey **(E)**. **(F, G)** Surface representation of the AexT homology model, colored according to the sequence conservation with ExoT **(F)** or ExoS **(G)**, respectively. Green indicates sequence identity; gold indicates similarity; grey indicates no conservation. Note the ridge of residues involved in target protein binding, running across the domain above the NAD^+ binding site (arrowheads); this region is identical in ExoT but unconserved in ExoS.

When coloring the individual amino acids according to the sequence conservation with ExoT and ExoS, a ridge of residues above the NAD^+ binding site becomes evident that is conserved with ExoT, but not conserved with ExoS (**Fig. 1F, G**). This ridge runs across the domain and includes residues that are part of regions B and C which were defined as low-homology regions by Sun et al.[26] Region B is within the active site loop and region C is also known as the ARTT loop in ADP-ribosylating toxins.[29] Together with two other regions, largely representing the PN-loop as well as the helix α1 (**Appendix Fig. 2D,** named according to Sun et al. 2004), those four regions were shown to play an essential role in the substrate specificity of ExoT.[26] Considering the high conservation between AexT and ExoT, but not ExoS, within those regions, we hypothesized that the ExoT and AexT ADP-ribosylating domains might be more similar in terms of their target spectrum than previously assumed. The *Pseudomonas* toxins have been studied and described extensively over the years. However, biochemical studies have always been challenging as the full-length proteins are difficult to purify. The same is essentially true for the less characterized AexT, which could only be purified from *E.coli* inclusion bodies so far.[11,23] Considering that the full-length toxins might have different enzymatic properties and therefore different target spectra compared to the ART domains, I decided to purify $AexT_{FL}$ and $ExoT_{FL}$ and compare them to their isolated ART domains.

The full-length toxins are aggregation-prone and difficult to express in *E.coli*

$ExoT_{FL}$ and $AexT_{FL}$ constructs were expressed in a canonical expression cell line (T7 express, NEB). $ExoS_{FL}$ and the ART domain of AexT ($AexT_{ART}$) were included as a reference for solubility. After cell lysis and clarification, the supernatants (soluble fraction) and the pellets (insoluble fraction) were analyzed via polyacrylamide gel electrophoresis (**Fig. 2A**). $AexT_{ART}$ can be purified in low yields from the soluble fraction. On the other hand, all full-length exotoxins are clearly overexpressed but found entirely in the insoluble fraction. To tune expression and solubility, the *Pseudomonas* ART domains can be expressed together with their host-derived chaperone 14-3-3β.[18] Therefore, I sub-cloned the AexT and ExoT full-length constructs into a 14-3-3β-containing co-expression plasmid. It has been shown that the interaction with 14-3-3β reduces the aggregation of the ART domains, thereby activating their enzymatic activities.[16] For that reason, ExoS:14-3-3β co-expression is toxic for *E.coli*.[18] This might explain why 14-3-3β co-expression leads to a reduced overall expression of $AexT_{FL}$ and $ExoT_{FL}$. In addition, the interaction with 14-3-3β is not sufficient to shift the toxins into the soluble fraction (**Fig. 2B**).

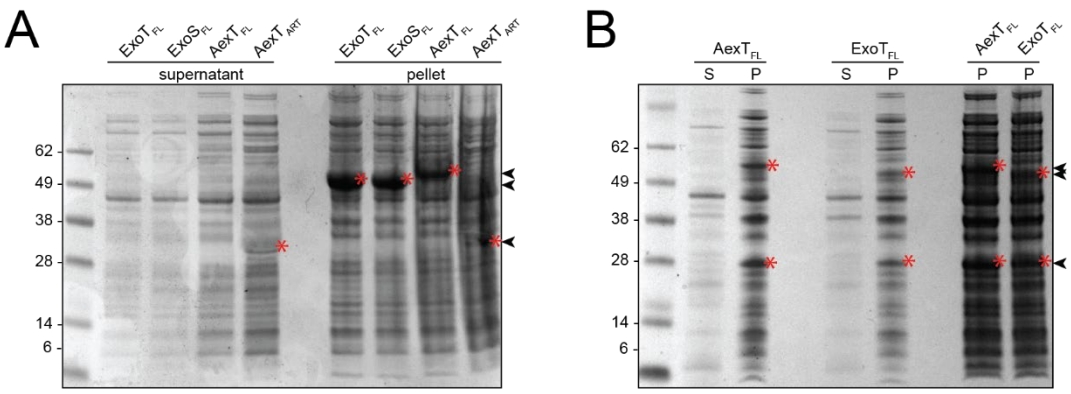

Figure 2 The Full-length toxins AexT, ExoT, and ExoS are insoluble when expressed in *E.coli*. Arrowheads indicate the approximate theoretical molecular weight of the constructs; asterisks indicate overexpression bands. **(A)** Standard expression of full-length toxins results in the accumulation of inclusion bodies. **(B)** Co-expression with the 14-3-3β chaperone does not improve solubility and in fact decreases expression, likely due to toxicity. The two lanes on the right correspond to a higher concentration of the same pellet fractions. S, supernatant; P, pellet. Details on experimental procedures are described in "Materials and Methods".

In an attempt to optimize the production of soluble protein, I screened various expression conditions. I tested different IPTG concentrations as well as inducer removal after induction. The theory behind inducer removal is that recombinant proteins are deposited in inclusion bodies during induction because the endogenous chaperones cannot handle the immense load of misfolded protein in the cell. When the inducer is removed, the expression of recombinant protein comes to a halt and chaperones regain the capacity of refolding misfolded proteins and bringing them back in solution. Another approach includes the addition of so-called osmolytes, small organic compounds that change the physical properties of the cell cytoplasm which is thought to have a positive effect on protein solubility. Bare addition to the culture medium is not enough for osmolyte uptake, which must be triggered artificially, for instance by the addition of salt. Finally, as with the 14-3-3β co-expression, exogenous chaperones are often utilized to assist in refolding, preventing aggregation, or even driving the re-folding of misfolded proteins. Instead of co-expressing specific chaperones, the artificial induction of a heat shock response can be used to trigger an overexpression of endogenous chaperones that might in turn prevent aggregation of recombinant proteins. One way of achieving this is by the addition of benzyl alcohol (methods adjusted from de Marco et al.).[30] None of the above-mentioned approaches had a positive effect on the expression or solubility of the $AexT_{FL}$:14-3-3β complex (**Appendix Fig. 3A**).

Testing different expression strains is common practice when optimizing expression conditions. I tested the expression of the full-length toxins from two different vectors, both as single expression and as 14-3-3β co-expression. The co-expression of the ART domains with 14-3-3β was tested alongside as a positive control. The amount of produced recombinant protein in the soluble and insoluble fractions was analyzed via SDS-Page, as shown for AexT (**Appendix Fig. 3B**) and for

two cell lines for ExoT (**Appendix Fig. 3C**). The expression of the ART domains in conjunction with 14-3-3β is low, but the complex can be purified with a good yield via immobilized metal affinity chromatography (IMAC; data not shown). As the ART domains have a similar molecular weight than 14-3-3β, it is difficult to distinguish two bands in the cell lysate. Even though co-expression results in better solubility, a substantial fraction of the ART:14-3-3β complex remains in the insoluble fraction, as seen for example in **appendix figure 3C**. When expressing the full-length toxins together with their chaperone, I could not identify a clear overexpression band, neither in the soluble nor in the insoluble fraction and in neither of the tested cell lines. Only expression of the full-length toxins without 14-3-3β resulted in an overexpression band in the right molecular size, which was more prominent in some of the cell lines (**Appendix Fig. 3B and 3C**, marked with a red asterisk). Although the expression of the full-length toxins can be tuned, I was unable to improve their solubility. Therefore, I decided to continue working with the best-expressing cell line (LEMO21 without the addition of L-rhamnose) and instead recover the proteins from the insoluble fraction, as it was done in other publications.[11,23]

Full-length AexT and ExoT can be successfully recovered from *E.coli* inclusion bodies

Recovery of proteins from inclusion bodies needs to be planned with care in order to circumvent the many pitfalls along the way. Parameters such as purity before refolding, the concentration of denaturant and potential additives, temperature, and protein concentration need to be assessed and monitored.[31–33] In the first step, the protein of interest is expressed in *E.coli* (here LEMO21, NEB) and the cells are lysed. It is of utmost importance that cell lysis is complete. Therefore, I used a rather harsh high-salt lysis buffer, supplemented with detergent, EDTA, benzonase, and lysozyme in addition to the canonical recipe (see Materials and Methods for details). The cell pellet was ruptured with a manual glass-glass homogenizer and the lysozyme reaction was allowed to proceed for 20 min at room temperature before sonicating repeatedly. Although inclusion bodies usually primarily consist of the protein of interest, other proteins, cell debris, and lipids may attach to them via hydrophobic interactions. Those contaminants can often be removed with several washes with a buffer containing low denaturant concentrations, such as ≤2 M urea and low concentrations of detergent.[31] **Figure 3A** shows the supernatants after several washing steps followed by centrifugation and illustrates that the purity of the inclusion bodies increased, but that the toxins were also partially solubilized. The toxins are the major component of the washed inclusion bodies. In the next step, the inclusion bodies were solubilized and the proteins were denatured with a high denaturant concentration (6.6 M guanidinium hydrochloride). The unsolubilized material was removed via centrifugation.

As contaminants can interfere with proper refolding, protein purity is a critical parameter.[31] Purification of the solubilized protein solution was challenging due to the high denaturant concentration. TALON columns for example could not withstand the high viscosity coming along

with the high denaturant concentration. I therefore decided to enriched the proteins of interest via batch purification with nickel-charged agarose beads (Ni-NTA beads). Unfortunately, guanidine also interferes with the binding to the beads, and conditions in which the His-tagged proteins bound to the beads needed to be established. Eventually, the majority of the protein did not bind to the beads and the purity after elution from the beads was only marginally improved (**Fig. 3B**).

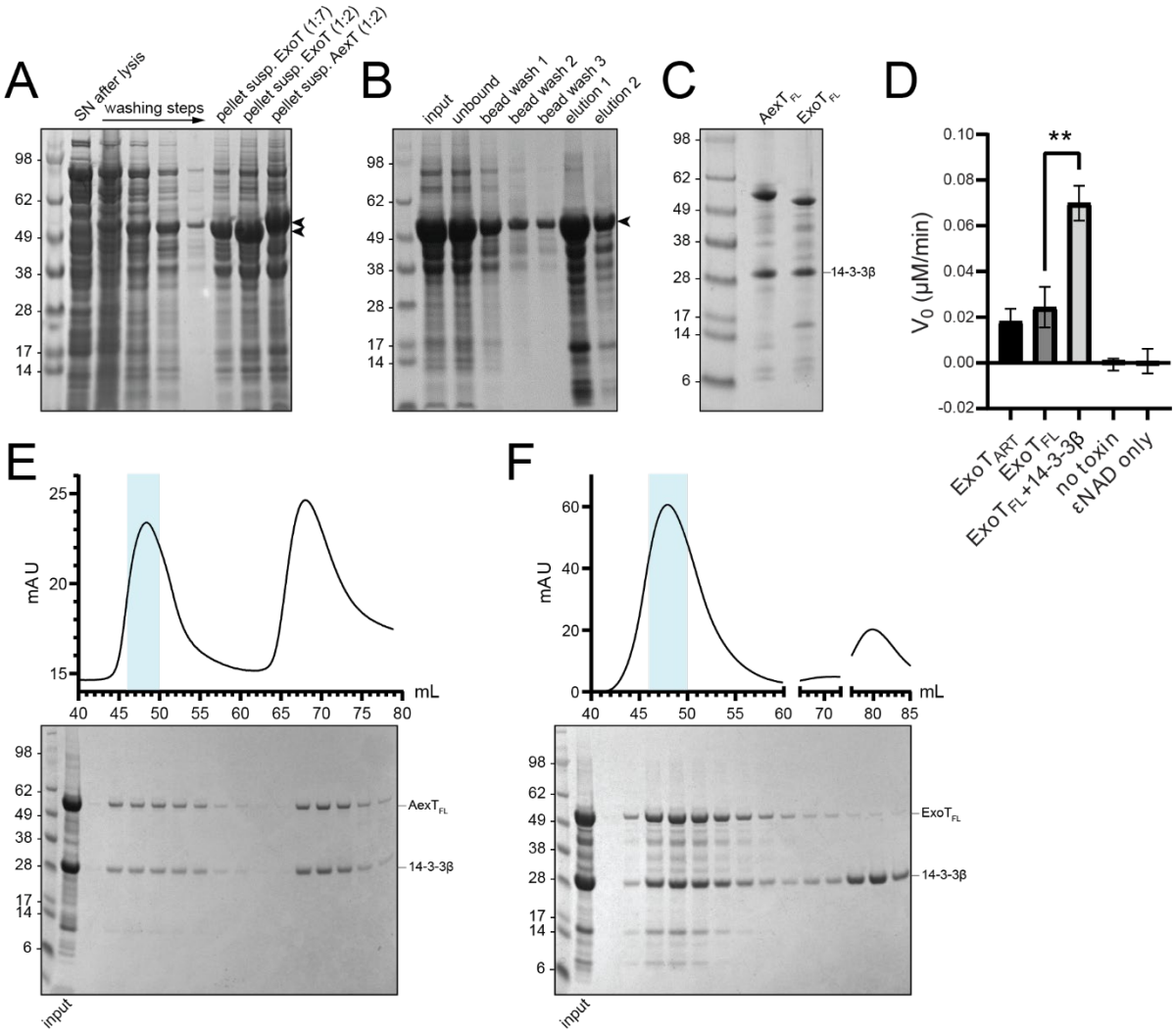

Figure 3 Steps in the recovery of full-length toxins from *E.coli* inclusion bodies. **(A-C)** SDS-Page gels illustrate the steps from cell lysis up to purified refolded proteins. **(A)** Cell pellets containing ExoT$_{FL}$ in inclusion bodies were subjected to multiple washing steps to remove contaminants (shown are the respective supernatants). The full-length toxins are the major components of the isolated inclusion bodies (pellet suspension in two different concentrations). The last lane shows isolated AexT$_{FL}$ inclusion bodies as a comparison. **(B)** The attempt of purifying denatured 6xHis-tagged ExoT$_{FL}$ with Ni-NTA beads results in low yield due to insufficient binding to the beads as well as poor improvement of purity. **(C)** Purified and refolded full-length toxins. 14-3-3β was added to the toxins during dialysis to assist in refolding. **(D)** The addition of 14-3-3β during the refolding process significantly improves the activity of refolded toxins. Processing rates were determined in an εNAD$^+$ assay with 200 nM toxin, 500 nM 14-3-3β, 5 μM CRK$_{SH2}$, and 40 μM εNAD$^+$. ******, adjusted P value = 0.002, determined with ordinary one-way ANOVA. **(D, E)** Further purification of AexT$_{FL}$- and ExoT$_{FL}$-14-3-3β complexes via gel filtration. A substantial amount of protein elutes in the void volume of the column (around 48 ml, indicated in blue; column: Hiload 16/600 Superdex 200 pg). The complex of interest elutes around 70 ml, followed by excess 14-3-3β.

There are several disputed theories about which parameters are essential and how they should be controlled to create the best environment for proper refolding. One of the most important but also intricate parameter is protein concentration. Most publications recommend using protein concentrations below 1 mg/ml, as aggregation propensity is always a function of concentration.[31] The protein concentration in the eluate from Ni-NTA beads was already below 1 mg/ml due to the low binding capacity. Refolding is generally initiated by the reduction of denaturant in solution. This can be achieved in different ways, such as dilution, dialysis, or on-column refolding.[31,32] Whether the denaturant concentration is to be decreased fast, slow, or in one or several steps is under discussion and might depend on the characteristics of the specific protein. Dilution was impractical as the volumes at this stage were already very large. Due to the high viscosity of the denatured protein solution and low binding capacity to metal-charged resins, on-column refolding was also unfavourable, which left us with dialysis as the remaining option. I aimed for a slow reduction of denaturant in solution which I achieved by step-wise dialysis.

The addition of so-called folding aids is a standard technique to improve refolding. Apart from small organic compounds that can be added to the dialysis buffer, chaperones are often used.[31,32] I decided to test the effect of 14-3-3β as a folding aid in the refolding process of the toxins. In the last dialysis step, before reducing the guanidine concentration from 0.5 M to 0 M, I added 14-3-3β in approximately equimolar concentrations.

Even though I attempted to control all the before-mentioned parameters, some protein aggregated during refolding. However, I found that the lower the total protein concentration, the less protein aggregated during refolding, consistent with the positive correlation between aggregation and protein concentration. The best results were obtained at a total protein concentration of 0.1 mg/ml. Nonetheless, aggregates had to be removed via centrifugation and filtration. Analysis of the aggregates via gel electrophoresis showed that mainly contaminants aggregated, leading to higher purity of the soluble fraction (data not shown). The purity of the refolded proteins was assessed via gel electrophoresis (**Fig. 3C**).

After refolding, it is necessary to determine whether the proteins refolded properly. This is generally straightforward for enzymes, as the enzymatic activity is an indication of correct folding. Other methods such as dynamic light scattering, circular dichroism, size exclusion chromatography, or native page can be used for proteins without enzymatic activity.[31] The activity of ADP-ribosylating toxins can be measured by the addition of 1,N^6-etheno-NAD^+ as a co-substrate. 1,N^6-etheno-NAD^+ (εNAD^+) is a NAD^+ analog with an etheno-moiety attached to the adenine, which confers fluorescence to the molecule. Following hydrolysis and displacement of the nicotinamide moiety, the fluorescence intensity increases 10-fold, and the intensity reaches the level of εAMP. Thus, εAMP can be used for calibration and therefore estimation of the amount

of εNAD$^+$ being processed by the enzyme.[34] As a positive control, I included the ExoT$_{ART}$:14-3-3β complex. As a negative control, toxin was omitted from the reaction. εNAD$^+$ alone does not show a change in fluorescence intensity with time (data not shown), indicating that both bleaching and spontaneous hydrolysis can be excluded. The analysis shows, that ExoT$_{FL}$ can be refolded without the addition of 14-3-3β, resulting in activity comparable to ExoT$_{ART}$. Nevertheless, the addition of 14-3-3β during the refolding process significantly increases the activity and thus the success in ExoT refolding (**Fig. 3D**).

As both ExoT$_{FL}$:14-3-3β and AexT$_{FL}$:14-3-3β were still contaminated, I aimed to purify them further. All contaminants appeared to be of lower molecular weights than the full-length toxins (**Fig. 3C**). The increased size difference upon complex formation with 14-3-3β made the samples applicable for size exclusion chromatography (SEC). The elution profiles in a Superdex 200 column as well as the analysis of the peak fractions in a polyacrylamide gel are shown in **figure 3** (panels **E** and **F** for AexT and ExoT respectively). A substantial fraction of the proteins eluted in the void volume. Together with the presence of many contaminants in the ExoT$_{FL}$:14-3-3β SDS-Page gel (**Fig. 3F**), it was to be assumed that the toxins aggregated. The presence of 14-3-3β in the aggregate peak indicated that not the full-length toxins alone but the toxin:chaperone complex aggregated. Nonetheless, AexT$_{FL}$:14-3-3β co-eluted in a pure second peak at around 70 ml. ExoT$_{FL}$:14-3-3β on the other hand was more prone to aggregation and only a very small fraction of the complex eluted at a similar elution volume, representing the soluble toxin:chaperone complex. After that, unbound 14-3-3β eluted from the column in a final peak. This pattern was observed in several subsequent purifications.

As the yield of refolded and functional protein after all those steps was very low, I decided to test a different strategy. The amount of protein that I could extract from the inclusion bodies was significantly high compared to what I could elute from Ni-NTA beads, implying a great loss of protein that remained unbound. Considering also the poor improvement in purity after batch purification, I set out to refold the proteins directly from the solubilized protein solution, without a preceding purification step. Although I observed a higher aggregation propensity when refolding at high protein concentrations, I hoped that most of the proteins that aggregate would represent contaminants. This would enable me to keep the volume low while increasing the yield further. The refolding procedure was essentially identical, but the complex was purified via IMAC and size exclusion chromatography after refolding. Whereas the purity was relatively comparable, the activity decreased slightly (data not shown), indicating again that high protein concentrations are less favourable for proper refolding.

Dynamic light scattering of size exclusion peaks reveals the proportion of aggregates in the population and serves as quality control for SEC-MALS

Interestingly, despite the evidence that peak 1 (void volume peak) in size exclusion chromatography of the full-length toxins represented aggregated toxin:chaperone complexes, I could measure activity by two different methods, using either εNAD$^+$ or biotin-NAD$^+$ as a co-substrate (data not shown). Therefore, I analyzed both size exclusion peaks of the AexT$_{FL}$:14-3-3β utilizing dynamic light scattering (DLS) (**Figure 4**). The speed of movement (Brownian motion) of particles in solution is dependent on their size. DLS measures this speed and can infer the diameter of the particles from that information, taking into account that a sphere with the same diameter would move at the same speed in the same solution. DLS is therefore an appropriate method to determine changes in the solubility of protein solutions and to detect aggregation. The standard depiction of the results is an intensity/size plot. However, as soon as there are multiple species in a population of particles, this depiction can be deceptive, because larger particles scatter more light than smaller particles, leading to higher intensities. That also means that the size of the peak is not proportional to the size of the population in solution. Transforming the data to a volume/size plot gives more information about the distribution of the populations, as the intensities are corrected for the volume of the particles. As the volume of aggregates is much larger than the volume of a simple protein complex, the peak area of the aggregates would be much higher than the peak area of the toxin:chaperone complex, if the population of both species were to be 1:1. Since the peak area of the smaller-sized population in **figure 4D** is much bigger, one can assume that in size exclusion peak 2 the toxin:chaperone complex is much more abundant than the aggregated fraction. On the other hand, **figure 4C** illustrates that size exclusion peak 1 contains more species that are bigger in size than expected from a simple toxin:chaperone complex (estimated hydrodynamic diameter of a complex consisting of one molecule AexT$_{FL}$ and two molecules 14-3-3β is ~8 nm; calculated with an online tool: www.fluidic.com). However, it is necessary to consider that the presence of a complex mixture of differentially sized particles creates problems with the inferred size estimation. Nevertheless, with DLS I could effectively distinguish aggregates from simple protein complexes.

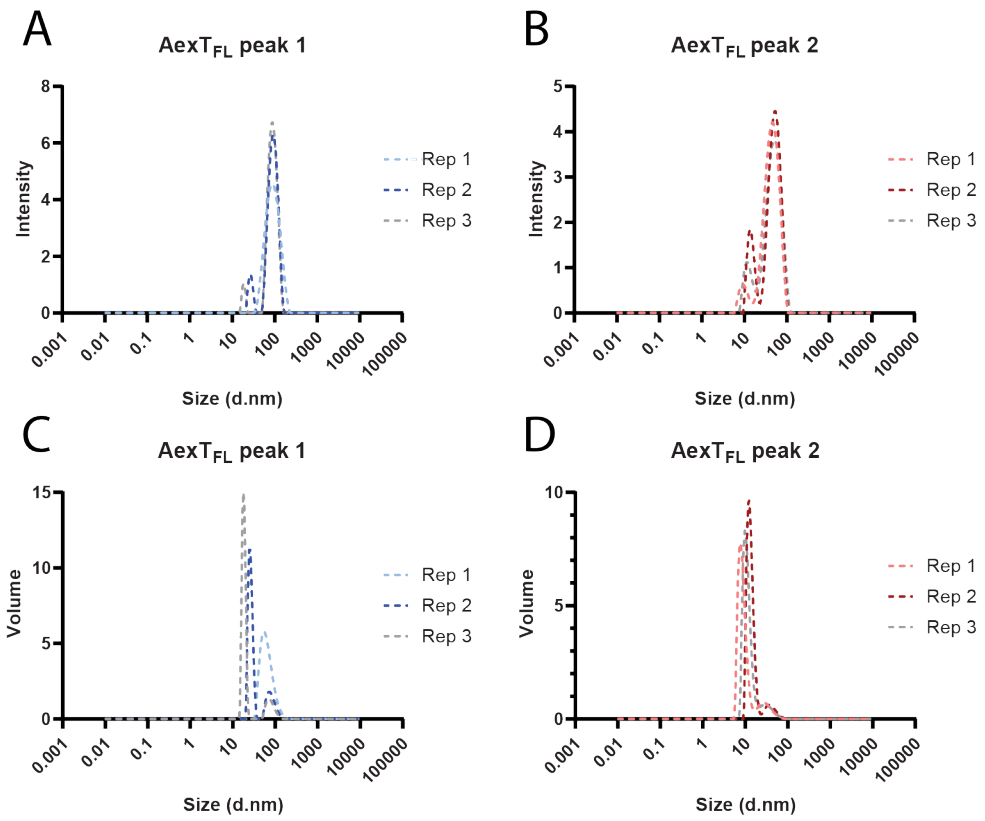

Figure 4 Dynamic light scattering reveals that AexT$_{FL}$:14-3-3β is aggregation-prone. Complex eluting in the void volume of the Superdex 200 pg column contains large aggregates **(A)**, which is more apparent in a volume/size plot **(C)**. AexT$_{FL}$ eluting in peak 2 also contains aggregates **(B)** which are however underrepresented in the population **(D)**.

ART domains form heterotrimeric complexes with 14-3-3β, in contrast to AexT$_{FL}$

AexT$_{ART}$ and ExoT$_{ART}$ behave better in solution, as seen by the reproducibility of DLS measurements (**Fig. 5A, B**). In both cases, a small peak appears just below 1 nm, which is too small to be a result of the scattering from proteins or peptides. We believe that this peak represents components in our buffer, eg. HEPES. When transforming to volume distribution, this peak is strongly overrepresented, making the protein peaks invisible. This is another indication that the peak derives from buffer components, as those are much more abundant than any macromolecule. As AexT$_{FL}$, the AexT$_{ART}$ and ExoT$_{ART}$ containing complexes form some aggregates that cannot be removed by centrifugation (>100 nm), but they are underrepresented compared to AexT$_{FL}$ (**Fig. 5C**).

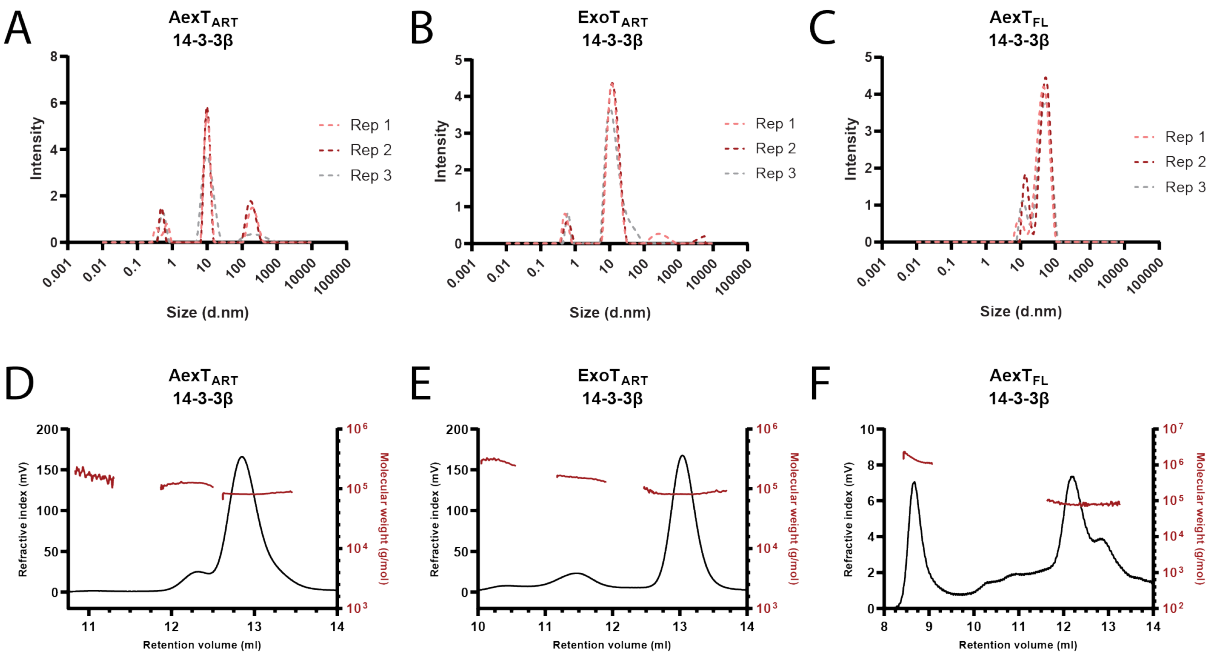

Figure 5 DLS (A-C) and SEC-MALS (D-F) profiles of the **(A, D)** AexT$_{ART}$:14-3-3β complex, **(B, E)** the ExoT$_{ART}$:14-3-3β complex, as well as **(C, F)** the AexT$_{FL}$:14-3-3β complex. Estimated molecular weights extrapolated from MALS are indicated in red **(D-F)**.

ExoT$_{ART}$ has previously been shown to form heterotrimers and heterotetramers with 14-3-3β dimers in solution.[18] The estimated hydrodynamic diameter of a heterotrimeric complex is 7.5 nm, which is smaller than the derived size obtained by DLS (**Fig. 5B**). As the derived size from DLS is only reliable in monodisperse samples, we decided to determine the molecular weight of the toxin:chaperone complexes via size exclusion coupled to multi-angle light scattering (SEC-MALS; OMNISEC system). Due to the high conservation with ExoT, we expected AexT$_{ART}$ to behave similarly to ExoT$_{ART}$. As the addition of the N-terminal part containing the GAP domain makes the toxins approximately two times larger and might potentially alter the overall conformation and constitution of the toxin:chaperone complex, we did not have any prior expectation from AexT$_{FL}$. Due to the formation of high-affinity homodimers of 14-3-3 molecules,[35] we predicted a behavior similar to that of the ART domain-containing complexes.

Although we could not infer precise sizes from DLS, the technique was useful to assess the quality of the protein samples before analyzing them via SEC-MALS. The DLS profiles of the samples analyzed are shown in **figure 5A-C**. As a control, I analyzed the ExoT$_{ART}$:14-3-3β complex in parallel. As expected from dynamic light scattering, both ExoT$_{ART}$ and AexT$_{ART}$ showed a good recovery and low dispersity. **Table 1** summarizes the most important data from the OMNISEC run. Most of the AexT$_{ART}$:14-3-3β complex (86,8%) eluted as a heterotrimer (**Fig. 5D**) with a measured molecular weight of 82 323 Da and a theoretical molecular weight of 84 571 Da. Less than 1% eluted in a polydisperse peak, which could potentially be contaminants. The rest was

present in a small shoulder that eluted just before the main peak and might represent a heterotetramer. In comparison, $ExoT_{ART}$:14-3-3β also eluted mainly as a heterotrimer (81,9%) with a measured molecular weight of 82 352 Da and a theoretical molecular weight of 83 757 Da. Two small peaks of 3,7% and 14,4% eluted earlier and had a good dispersity value. However, at high estimated molecular weights it is difficult to infer their composition. The first peak could be a decamer, whereas the second and bigger peak could represent a hexamer. A similar pattern has been observed by Karlberg et al.[18] $AexT_{FL}$:14-3-3β had a very low recovery, indicating that much of the complex aggregated before injection into the column and was removed through filtration. Of the small amount of protein that was injected, 30% eluted in the void volume as a consequence of aggregation that formed just before injection or during the run. This might be triggered additionally due to the lack of glycerol in the running buffer, which would interfere with the viscosity measurement. Nevertheless, 71% eluted in a deformed peak with a right shoulder. The molecular weight is identical in both, peak and shoulder, and has a good dispersity value. To our surprise, the extrapolated molecular weight (81 901 Da) is very close to the theoretical molecular weight of a dimer (82 014 Da), consisting of one 14-3-3β and one $AexT_{FL}$ molecule. This is surprising as most 14-3-3 containing complexes are formed by homo- or heterodimers of the chaperone, although certain conditions such as phosphorylation favour the disassembly of 14-3-3 dimers.[35] $ExoT_{FL}$ complex organization could not be tested in SEC-MALS analysis due to a shortage of soluble protein.

	$AexT_{ART}$:14-3-3β			$ExoT_{ART}$:14-3-3β			$AexT_{FL}$:14-3-3β	
	Peak 1	Peak 2	Peak 3	Peak 1	Peak 2	Peak 3	Peak 1	Peak 2
Retention volume (mL)	11.06	12.45	12.85	10.43	11.46	13.04	8.67	12.19
Molecular weight (g mol^{-1})	165 789	122 560	82 323	287 849	153 539	82 352	1 439 034	81 901
MW at peak apex (g mol^{-1})	160 420	105 342	81 630	275 819	158 165	81 783	1 439 034	77 634
Theoretical MW (g mol^{-1})	*27 503* *28 534*	*27 503* *28 534*	*27 503* *28 534*	*26 689* *28 534*	*26 689* *28 534*	*26 689* *28 534*	*52 658* *29 356*	*52 658* *29 356*
Dispersity (MW/MN)	1.022	1.003	1.001	1.007	1.003	1.001	1.035	1.006
Fraction of sample	0.9%	12.4%	86.8%	3.7%	14.4%	81.9%	29%	71%
Recovery	104%	104%	104%	94%	94%	94%	10.5%	10.5%
Inferred complex composition (14-3-3β:toxin ratio and expected MW)	Too polydis-perse	Tetramer* (2:2; 112 074 Da)	Trimer (2:1; 84 571 Da)	Decamer* (5:5; 276 115 Da)	Hexamer* (3:3; 165 669 Da)	Trimer (2:1; 83 757 Da)	Aggre-gates	Dimer (1:1; 82 014 Da)

Table 1 Summary of SEC-MALS (OMNISEC) analysis of $AexT_{ART}$, $ExoT_{ART}$, and $AexT_{FL}$ in complex with 14-3-3β. Retention volume refers to the peak maximum. Molecular weight is given as the weight average from the molecular weight distribution of each peak. Theoretical molecular weight was calculated with the webtool expasy.org. The polydispersity index is given by MW/MN, where MN is the number average molecular weight from the molecular weight distribution. The fraction of sample is defined for each peak, expressed as percent of the total area of all the analyzed peaks together. Definitions are adjusted from the OMNISEC system User Guide (MAN0550-06-EN). *ambiguous inferred complex composition.

AexT and ExoT enzymatic activity and specificity are comparable

All purified toxin:chaperone complexes were enzymatically characterized in εNAD⁺ assays (**Fig. 6**). Without the addition of substrates, the processing rates are generally very low as they exclusively emerge from the hydrolysis of εNAD⁺. Through titration of the co-substrate εNAD⁺, I could fit the data to Michaelis-Menten curves to determine the apparent Km values. For all toxin variants, the Km for εNAD⁺ is in the low micromolar range (**Table 2**). However, the processing rates of the full-length toxins are consistently higher than those of the respective ART domains.

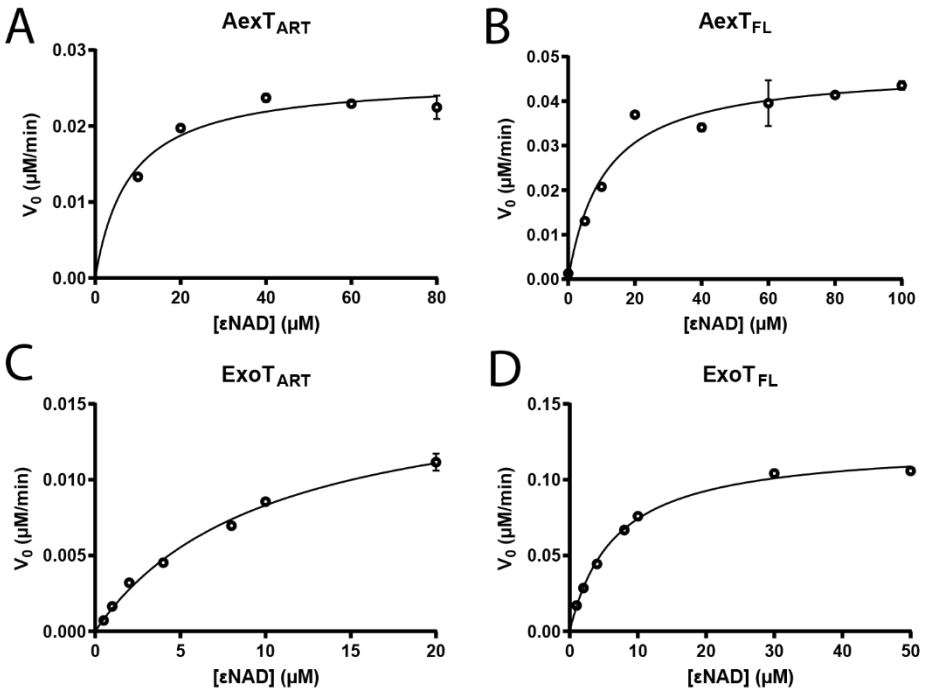

Figure 6 Enzymatic activity of the ART domain and full-length variant of AexT (A, B) and ExoT (C, D), respectively. Enzymatic activities in dependence of εNAD⁺ concentration were determined and Michaelis Menten constants were calculated in GraphPad PRISM (see Materials and Methods for details). The absence of substrates results in low, but measurable activity. The Km values reside in the low micromolar range (refer to **Table 2**). Note that the processing rates of the full-length toxins are consistently higher than those of their respective isolated ART domains. n = 3, error bars show the standard error from the mean.

construct	substrate	K_M (µM)	V_{max} (µM min^{-1})	k_{cat} (min^{-1})	k_{cat}/K_M ($µM^{-1}min^{-1}$)
$AexT_{ART}$	(εNAD⁺)	8,06 ± 1,47	0,03 ± 0,00	0,13	1,6E-02
	Agmatine	5084 ± 159	0,79 ± 0,01	3,959	7,8E-04
$AexT_{FL}$	(εNAD⁺)	10,94 ± 1,99	0,05 ± 0,00	0,235	2,1E-02
	Agmatine	6648 ± 467	1,41 ± 0,05	7,05	1,1E-03
$ExoT_{ART}$	(εNAD⁺)	10,08 ± 1,04	0,02 ± 0,00	0,085	8,4E-03
	Agmatine	3379 ± 157	0,67 ± 0,02	3,37	1,0E-03
$ExoT_{FL}$	(εNAD⁺)	6,57 ± 0,24	0,12 ± 0,00	0,615	9,4E-02
	Agmatine	2193 ± 126	3,01 ± 0,07	15,025	6,9E-03

Table 2 Michaelis-Menten kinetic constants determined in εNAD⁺ assays. Details on reaction compositions are given in the Materials and Methods section. εNAD⁺ is in parentheses as it is not considered a substrate. Km for εNAD⁺ can be determined because toxins exhibit low but measurable NAD-hydrolysis activities.

As the two orthologs proved to be very similar in the previous experiments, we now decided to investigate their target spectrum. The best-described substrates are actin and CRK, for AexT and ExoT respectively. In the first assay, I tested the enzymatic activity over *Bos taurus* β-actin (**Fig. 7A**). To discriminate between target and auto-modification, I performed reactions with biotinylated NAD^+ that were subsequently subjected to gel electrophoresis. The separated proteins were transferred onto a PVDF membrane and biotin-ADP-ribosylation was detected using HRP-conjugated streptavidin (refer to Materials and Methods for details). The *Clostridium botulinum* C2I toxin subunit was used as a positive control for actin modification[36] and the human mono-ADP-ribosyltransferase PARP10 was used as a control for auto-modification.[37] As expected, β-actin is modified by $AexT_{ART}$ and to a lesser extent by $AexT_{FL}$. The reduced activity of the full-length variant over β-actin might be explained by the auto-modification of $AexT_{FL}$, which has not been described before.[11] If the affinity for other $AexT_{FL}$ molecules is higher than for β-actin, a competing mechanism for the substrate might explain the reduced activity towards β-actin. $ExoT_{FL}$ on the other hand is known to undergo auto-modification[9], which can clearly be seen in the protein overlay assay (**Fig. 7A**, right panel).

To our surprise, β-actin was also modified by both variants of ExoT. Interestingly, $ExoT_{FL}$ seems to be more competent in modifying β-actin compared to the isolated ART domain, which is contrary to its orthologue AexT. However, it must be kept in mind that protein overlay assays are merely a qualitative method and cannot be used for precise quantitative measures. Both full-length toxins seem to marginally modify 14-3-3β, which cannot be clearly stated for the isolated ART domains.

With this new information in mind, I decided to incubate the toxins with human leukemia cell lysates (Jurkat E6.1 cell line; **Fig. 7B**). This would give us an indication of the specificity of the toxins as well as whether actin from cell lysates is also modified. For AexT, the pattern of modified substrates in cell lysates resembles very much the reactions containing the purified components. No additional and specific proteins appear to be modified in the lysate. Reactions with ExoT are more complex to interpret, as incubation of the lysate with the full-length toxin results in high background levels. Nevertheless, $ExoT_{ART}$ is clearly able to modify actin extracted from Jurkat cells. ExoT has been shown to modify the proteins CRK-I, CRK-II, and PGK-1.[9] No modification of those proteins can clearly be detected in the protein overlay assay, which can presumably be explained by the above-average concentration of actin compared to most other proteins in mammalian cells. Whether the high background in the case of $ExoT_{FL}$ is a result of a higher substrate spectrum compared to $ExoT_{ART}$ or simply results from the higher enzymatic activity remains to be tested. As expected, the positive control C2I is specific for actin.

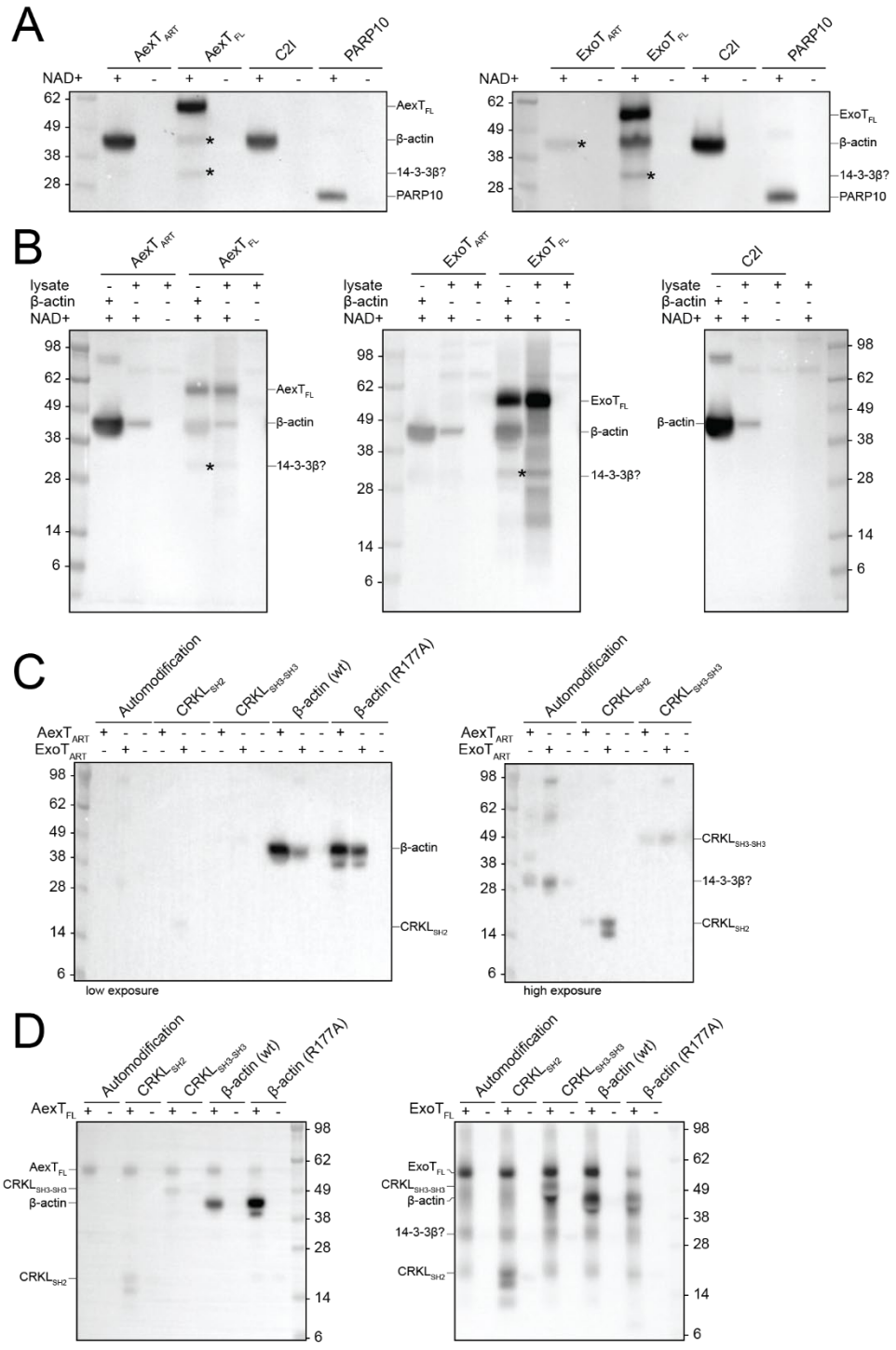

Figure 7 Protein overlay assays show that AexT and ExoT have a common target spectrum. (A) Modification of isolated β-actin as well as auto-modification of the different toxin constructs. *Clostridium botulinum* enzyme subunit C2I and human PARP10 serve as positive controls of actin- and auto-modification, respectively. **(B)** Actin is also modified in Jurkat cell lysate when incubated together with the toxins. **(C,D)** R177 is likely not the only residue in β-actin that is modified by the ART domains (**C**) or the full-length toxins (**D**). The known substrate of ExoT, CRK, is only marginally modified compared to actin, the signal being almost at the level of the background. The concentration of $ExoT_{FL}$ was reduced to 500 nM to reduce the background signal. Substrate concentrations are 10µM each.

Both ExoT and AexT ADP-ribosyltransferase activity was found to be directed towards arginine residues in their respective substrates.[11,38] AexT was shown to modify actin at a single arginine residue in position 177.[11] To test whether ExoT is also specific for this residue, I performed ADP-ribosylation reactions with a β-actin variant that was mutated at position 177 (β-actin R177A; **Fig. 7C, D**). CRK is modified on arginine 20 in its SH2 domain by ExoT[38], which is conserved in CRK-like protein (CRK-L). I therefore screened for modification of the CRK-SH2 domain by AexT and ExoT and included a GST-tagged construct of the two SH3-domains of CRK-L as a negative control. At low exposure of the ART domain-containing membrane, a strong signal appeared at the position of actin (**Fig 7C**, left panel). To our surprise, the actin mutant lacking R177 was modified by all four toxin variants (**Fig. 7C, D**). In the case of $ExoT_{ART}$ and $AexT_{FL}$, modification of the mutant appears to be more efficient than of the wild-type variant. Those results indicate that R177 is not the only amino acid in actin that is ADP-ribosylated by the toxins. CRK SH2 domain modification by $ExoT_{ART}$ became only visible after longer exposure (**Fig. 7C**, right panel). Additional weak signals appeared in reactions with $AexT_{ART}$ + CRK_{SH2} and reactions containing $CRKL_{SH3\text{-}SH3}$. This finding suggests that AexT has a low activity over CRK and that the SH3 domains of CRKL might also be ADP-ribosylated by the toxins. However, the high exposure of the membrane already reveals background signal in control reactions that is of similar intensity to the bands in question, which is why this interpretation cannot be unambiguously made. In reactions with the full-length toxins, modification of the substrate variants is more evident. However, the high background signal of $ExoT_{FL}$ is again problematic in terms of result interpretation.

Arginine-specific modification of actin inhibits its polymerization *in vitro*

The experiments with the actin R177A mutant raised the question of whether the toxins are arginine-specific or whether other residues might be modified. First, I tested whether arginines are acceptor residues of the toxins by utilizing the decarboxylated arginine analog agmatine as an acceptor in εNAD^+ assays[34] (**Fig. 8A-D**). As agmatine is not a natural substrate for the toxins, high Km values were expected (mM range; refer to **Table 2**). Notably, the processing rates of all four toxin variants were boosted 20- to 70-fold with the addition of the artificial substrate. Agmatine alone did not result in any change in fluorescence intensity (data not shown). This experiment illustrates that arginines are acceptor residues for ADP-ribosylation by AexT and ExoT. To show that the toxins are also specific for arginines, I performed auto-ADP-ribosylation reactions of $AexT_{FL}$ and $ExoT_{FL}$ followed by the addition of residue-specific ADP-ribosylhydrolases and detected the remaining ADP-ribosylations in a plate-based method utilizing an engineered GFP-fused macrodomain[39] (refer to Materials and Methods for details). Interestingly, $ExoT_{FL}$ without the addition of NAD^+ already showed some background signal (**Fig. 8F**), indicating that it might already be moderately modified during expression in *E.coli*, which is conceivable due to the low

Km for εNAD$^+$ (**Table 2**). The arginine-specific ADP-ribosylhydrolase ARH1[40] was able to remove most auto-modifications of $AexT_{FL}$ and $ExoT_{FL}$ (**Fig. 8E, F**). MacroD2, which is specific for the removal of ADP-ribose from glutamic and aspartic acids[41] is inefficient to remove ADP-ribosylations from the toxins. The reduced signal in reactions with the serine-specific ARH3[42] might represent an artifact, which is supported by the following observations; (i) the combination of ARH1 and ARH2 does not result in a complete loss of ADP-ribose, but instead shows an intermediate effect, (ii) the addition of free ADP-ribose after the hydrolase reaction increases the signal in reactions with ARH3, but not with ARH1 and (iii) no signal reduction can be seen in preliminary protein overlay assays (data not shown). Collectively, those observations indicate that ARH3 might be able to bind, but not cleave the ADP-ribose moieties attached by the exotoxins. Instead, the observed signal decrease might result from insufficient removal of ARH3 by competition with free ADP-ribose, which in turn potentially shields the attached ADP-ribose moieties from detection by the GFP-fused macrodomain. On the other hand, the addition of free ADP-ribose to ARH1 treated wells does not change the signal intensity, indicating that ARH1 effectively hydrolyses arginine ADP-ribosylation and detaches thereafter.

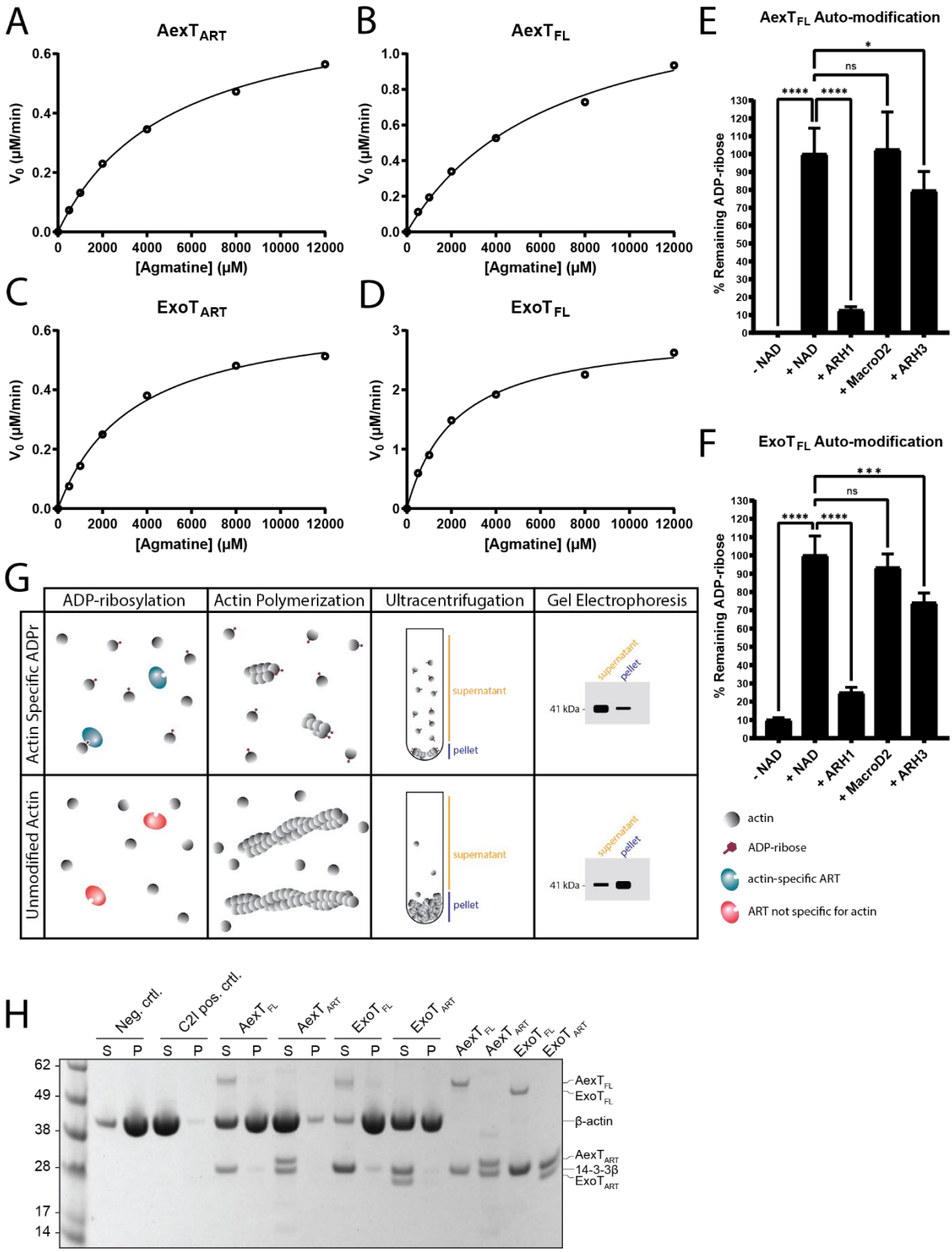

Figure legend on next page.

Figure 8 AexT and ExoT residue specificity and the effect on actin polymerization. (A-D) εNAD$^+$ assays with titrations of an artificial substrate, the arginine analog agmatine, shows that arginines are ADP-ribosylated by the toxins, thereby boosting the processing rates. n = 3, error bars cannot be depicted, standard errors are too small. **(E, F)** The arginine-specific ADP-ribosylhydrolase ARH1 removes most $AexT_{FL}$ **(E)** and $ExoT_{FL}$ **(F)** auto-modifications, in contrast to MacroD2. The reduction with ARH3 might be an artifact of the method (see text for more details). Error bars depict the standard deviation from the mean; n=8. Significance was tested with Welch ANOVA test with P > 0.05 (ns), P ≤ 0.05 (*), P ≤ 0.001 (***), P ≤ 0.0001 (****). **(G)** Principle of the actin polymerization assay. **(H)** The modification of actin impairs its polymerization *in vitro*. The effect of ADP-ribosylation deposited by ART domains is stronger than that of the full-length equivalents. S, supernatant; P, pellet.

Having evidence that $AexT_{FL}$ and $ExoT_{FL}$ are indeed arginine-specific, I tested whether the modification of β-actin would interfere with actin polymerization *in vitro*. Modifications on R177 of actin have been described to inhibit actin polymerization, as this residue is positioned at the interface between adjacent actin monomers in the polymer. ADP-ribosylation at this site sterically prevents the addition of actin monomers to actin filaments.[7] To test whether AexT and ExoT-deposited ADP-ribosylation on actin would interfere with its polymerization, I triggered the polymerization of ADP-ribosylated actin by the addition of KCl and $MgCl_2$. Actin modification by *Clostridium botulinum* C2I served as a positive control. For negative controls, toxins were omitted. Actin polymers were pelleted by ultracentrifugation and pellet and supernatant fractions were analyzed via gel electrophoresis. In negative controls, actin polymerization can occur unhindered, resulting in a large number of actin molecules incorporated in polymers which are subsequently pelleted by ultracentrifugation. On the other hand, if enough actin molecules are ADP-ribosylated at the interaction interface, polymerization will be largely impeded and the majority of actin molecules will stay as monomers in the supernatant (**Fig. 8G**). This effect can be illustratively observed by C2I-catalyzed actin modification (**Fig. 8H**). The full-length toxins seem to have limited effects on actin polymerization, although a small shift of actin into the supernatant can be observed in the reaction containing $AexT_{FL}$. The effect of the ART domains on actin polymerization is more apparent. Whereas $ExoT_{ART}$ is able to shift approximately half of the actin molecules into the supernatant, $AexT_{ART}$ is able to do that with almost all the molecules. Those results are mostly consistent with the protein overlay assays depicted in **figure 7B**. We can conclude that AexT and ExoT are arginine-specific ADP-ribosytransferases that inhibit actin polymerization *in vitro*. Actin might be modified on other residues apart from R177. Whether the modification of other arginines within actin has an impact on actin polymerization needs further investigation. Mass spectrometry analysis will give us new insights into the ADP-ribosylation of actin by 14-3-3 dependent bacterial toxins.

DISCUSSION

Pseudomonas aeuroginosa and *Aeromonas salmonicida* are two pathogenic bacteria belonging to the class of gammaproteobacteria and are therefore phylogenetically closely related. Whereas *A.salmonicida* infections cause furunculosis in fish[13,14], *P.aeruginosa* is a human pathogen that is infamous for causing life-threatening secondary infections in immunocompromised individuals.[6] Despite their different hosts, both pathogens share several of their infection strategies, including the injection of exotoxins directly into the host cell cytoplasm via the type three secretion system.[6,12] Previous studies found that ExoS and ExoT of *P.aeruginosa* and AexT of *A.salmonicida* are orthologous toxins that cause similar morphological changes in infected cells.[10,23] Closer investigations confirmed that their mechanism of action is also similar and dependent on a GTPase activating protein (GAP) domain and an ADP-ribosyltransferase (ART) domain. Whereas the GAP domains of all three toxins target the same host proteins, the specificity of the ADP-ribosylating domains differs.[11,16] Our computational analysis showed that the ART domains of the toxins are better conserved than the GAP domains, which seemed counterintuitive regarding their substrate specificities. With the help of an $AexT_{ART}$ homology model, we found that AexT shares more structural features with ExoT than with ExoS, suggesting a similar ART domain target spectrum. In addition, a hydrophobic patch on the C-terminal part of the model presumably represents the binding site of its putative host-derived chaperone 14-3-3.

The $AexT_{ART}$ model indicates a well-folded structure reminiscent of the conserved ART fold.[2] $AexT_{ART}$ can successfully be purified from the soluble fraction, with higher yields when co-expressed with 14-3-3β. The full-length toxin is approximately twice the size and comprises a GAP domain as well as several other motifs that are predicted to be disordered (**Appendix Fig. 2E**). Therefore, it is not surprising that neither $AexT_{FL}$ nor $ExoT_{FL}$ can be purified from the soluble fraction in *E.coli*. I showed that altering the expression conditions can affect the expression level, but not the solubility of the toxins. Co-expression with 14-3-3β did not have a positive effect on expression or solubility, which might be connected to inferred toxicity as proteins of the 14-3-3 family are known to activate the toxins.[4,16] In fact, $ExoS_{ART}$ catalytic residues had to be mutated to eliminate the toxicity in *E.coli*.[18]

Previous studies on the toxins faced similar problems and therefore the authors decided to use alternative methods to obtain proteins for biochemical analysis. While some triggered *P.aeruginosa* to secrete the toxins into the surrounding medium[9], others recovered them from *E.coli* inclusion bodies.[11,23] The analysis of the insoluble fraction in my experiments showed that under certain conditions the toxins are highly expressed but are incorporated into inclusion bodies. Combining different protocols and performing extensive optimization, I successfully managed to recover $ExoT_{FL}$ and $AexT_{FL}$ from inclusion bodies. Enzymatic assays confirmed correct refolding. 14-3-3 turned out to significantly improve the success of refolding and was

therefore included by default in subsequent purifications. My results indicate that 14-3-3 decreases the aggregation propensity of the full-length toxins, as was already demonstrated with the *P.aeruginosa* ART domains.[18] Size exclusion chromatography, dynamic light scattering, and SEC-MALS analysis showed that the toxins are highly aggregation-prone, even in complex with 14-3-3β. However, aggregated fractions still exhibited considerable activities as tested with εNAD^+ and protein overlay assays. Those observations might be connected to a dynamic exchange of soluble molecules with high molecular weight aggregates. An alternative explanation might be the formation of high molecular weight complexes, as has been proposed by Karlberg et al. In crystal structures of $ExoS_{ART}$ in complex with 14-3-3β the authors found that in heterotrimeric complexes the second LDLA box of $ExoS_{ART}$ was placed in the phosphoprotein binding site of the 14-3-3β monomer with a free substrate binding site. This observation might be part of a regulatory mechanism in which the phosphoprotein binding site in 14-3-3 acts as a sensor for toxin concentration in the host cell cytoplasm. As the number of toxin molecules increases, the second LDLA box might be replaced by an LDLA-box1 of another ExoS molecule to form a tetrameric complex, making the two C-terminal LDLA-boxes of the two ExoS molecules accessible for binding by another 14-3-3 molecule.[18] Higher-order complexes formed by such a mechanism would also explain the high molecular weight species found in our SEC-MALS analysis as well as in previous analyses of $ExoS_{ART}$:14-3-3β and $ExoT_{ART}$:14-3-3β complexes.[18] The molecular weights found in those experiments are poorly reproducible among different runs but are always relatively concordant with the theoretical molecular weights of higher-order complexes, such as hexamers or decamers. Considering the well-described tight interaction between 14-3-3 dimers of several isotypes, including 14-3-3β, we were surprised that the only monodisperse species detected by OMNISEC analysis of the $AexT_{FL}$:14-3-3β complex is indicative of a heterodimer consisting of one 14-3-3β and one $AexT_{FL}$ molecule. Although 14-3-3 family proteins are known to form high-affinity homo- and heterodimers, approximately 30% are present in the monomeric form *in vivo*, representing a monomer-dimer equilibrium. Under certain conditions, such as phosphorylation at serine 58, 14-3-3 dimers are prone to disassemble. 14-3-3 mutants incapable of dimerization have also been reported to possess higher chaperoning capabilities, likely due to an additional hydrophobic surface that is exposed where the second 14-3-3 monomer would bind.[35] Considering that a substantial part of the toxins, i.e the N-terminal region before the GAP domain, lacks a predicted secondary structure and is mainly apolar (**Appendix Fig. 2E, F**), it is conceivable that this part folds back onto the hydrophobic interface, thus displacing the second 14-3-3 molecule from the dimer. Whether the interaction with $AexT_{FL}$ might indeed in some way interfere with the binding of a second 14-3-3 monomer remains to be examined. Additional structural analyses will create a clearer picture of the toxin:chaperone complexes existing *in vitro*.

Despite the high aggregation predisposition of the full-length toxins, especially of ExoT, I could measure enzymatic activity and I was able to determine the Km for εNAD$^+$. Compared to the isolated ART domains, the full-length toxins have a similar affinity for εNAD$^+$, suggesting that the presence of the N-terminal part of the toxins does not alter the conformation of the NAD$^+$ binding site. Notably, the processing rates of the full-length toxins are higher compared to the ART domains. This observation is likely connected to the auto-modification of the full-length toxins, which seems to be absent in ART domains, as shown in the protein overlay assays. On the other hand, the ART domains alone seem to merely hydrolyse εNAD$^+$, but do not attach ADP-ribose in the absence of substrate. Although ExoT has been previously described to modify itself, as has ExoS,[16] AexT has been reported to lack auto-modification activity.[11] The absence of auto-modification in $AexT_{ART}$ and $ExoT_{ART}$ suggests that ADP-ribose is exclusively attached to target residues outside of the ART domain, or, that the N-terminal parts offer structural support to enable auto-modification. In fact, ExoS has been shown to auto-modify the catalytic arginine of its own GAP domain, thereby down-regulating its GTPase activating activity.[43] A similar mechanism might be used to regulate the GAP activity of AexT and ExoT. Which residues are auto-ADP-ribosylated will be revealed by mass spectrometry analysis.

Our homology model of $AexT_{ART}$ illustrated that regions that are believed to confer substrate specificity are conserved with ExoT but different from ExoS. This finding suggests that the target spectrum of AexT and ExoT might be more similar than previously described. Indeed, I found that the well-known targets of AexT and ExoT, actin and CRK respectively, are in fact common targets of both toxins. So far, ExoT and AexT ADP-ribosylating activities were believed to alter the integrity of the cytoskeleton of infected cells through two different mechanisms. AexT was thought to exclusively modify actin on R177, thereby introducing a cumbersome moiety at the interface between actin monomers, which would eventually result in the depolymerization of actin filaments.[11] On the other hand, ExoT was described to have an indirect, upstream effect on the actin cytoskeleton. The ADP-ribosylation of CRK and CRKL inhibits binding events within the signaling cascade that normally leads to Rac1 activation, consequently preventing phagocytosis activation.[38] Why actin, although being one of the most abundant proteins in mammalian cells, was never before identified as a target of ExoT is not clear. In fact, Sun and Barbieri detected additional targets in CHO cells that were not further characterized.[9] Here I show that ExoT and AexT have direct effects on the cytoskeleton by ADP-ribosylating actin as well as indirectly by the modification of CRK proteins.

Arginine at position 177 has been identified as the only residue in actin that is modified by AexT.[11] Due to the high similarity to ExoT, we hypothesized that the same residue is modified by the *P.aeruginosa* ortholog. Protein overlay assays with an actin mutant, in which arginine 177 is replaced by alanine, indicated that R177 is not the only residue being modified. In some cases,

the mutant seemed to be a better substrate for the toxins than wild-type actin. This might be explained by the decreased polymerization capability of actin mutated at R177.[44] Arginine 177 sits on the interface between adjacent actin monomers in the filament.[7] Therefore, replacement by the smaller and apolar alanine residue impairs the formation of polymers, whereupon more monomers will be in solution and available for interaction with the toxins. Subsequent experiments confirmed that arginine is a target for both toxins, in their full-length as well as truncated forms, and that arginines are likely to be the only acceptor residue type. Whether others of the eighteen arginines in actin are modified by the toxins will be revealed by a currently awaiting mass spectrometry analysis. Meanwhile, I could show that the toxins effectively inhibit actin polymerization *in vitro*. Why the full-length toxins are less effective than their respective ART domains is not clear. $ExoT_{FL}$ is the toxin with the least effect on actin polymerization and at the same time the toxin with the highest processing rates which possibly results from extensive auto-modification. Confirmed by protein overlay assays, ExoT molecules seem to be a preferred target over actin, which means that the ART activity of ExoT is mainly directed towards other ExoT molecules. If the concentration of ADP-ribosylated actin is below the critical concentration for actin polymerization, the effect of ExoT on actin polymerization will be negligible, making this assay inappropriate to detect actin ADP-ribosylation.

At the same time, we cannot exclude the possibility that the auto-ADP-ribosylation of the full-length toxins downregulates their own ADP-ribosylating activity. This in turn might represent another layer of regulation of unknown effects *in vivo*. Both *P.aeruginosa* and *A.salmonicida* infection strategies primarily rely on the evasion of the host immune system. The combined effect of the GAP and ART activities leads to cell rounding, weakening of tight and adherent junctions, and inhibition of phagocytosis,[4,7,8] but ExoT has been described to be non-cytotoxic (i.e. not inducing cell death).[16] Negative autoregulation might therefore be essential to keep that balance. In accordance with this hypothesis, artificially extended infection with the toxins has been shown to lead to cell death.[4,23]

In conclusion, through biochemical and computational characterization we found that AexT and ExoT are highly similar. In conjunction with previous studies that showed that Rho, Rac, and Cdc42 are targets of the GTPase activating activities of the two orthologs,[11,20] I found that also their ART domain target spectrum overlaps. Therefore, both toxins have the ability to affect the host cell cytoskeleton through two different mechanisms. On the one hand, the activation of Rho GTPases has an upstream regulatory effect, leading to cytoskeleton breakdown which results in cell rounding and disorganization of tight and adherence junctions. The ADP-ribosylation of actin has a similar effect, however more direct. The modification of upstream regulators such as CRK guarantees the disruption of the signaling cascade leading to phagocytosis. This also explains the similar morphological changes of cells infected by ExoT or AexT, and why the mutation of

either of the two domains separately is not enough to prevent the concomitant phenotype.[11,15] Together, the two domains of the bifunctional toxins individually manipulate the integrity of the host cell and weaken it on different layers, leading to the same overall goal, evasion of the immune system and dissemination within the host.

MATERIALS AND METHODS

$AexT_{ART}$ structural homology model

The AexT, ExoT, and ExoS sequences were downloaded from Uniprot (accession numbers Q93Q17, Q9I788, and G3XDA1, respectively) and aligned in Jalview with the ClustalO algorithm. The final alignment figure was produced in the Espript 3.0 browser tool. Given the sequence similarities within the ART domains, we used ExoT as a template to model the $AexT_{ART}$ structure (comprising residues 255-452; AexT numbering). The model was built with SWISS-MODEL[28], using the previously published structure of an $ExoT_{ART}$:14-3-3β heterotetramer (PDB: 6GNN)[18] as a template. The inhibitor STO1101 (3-(12-oxidanylidene-7-thia-9,11-diazatricyclo[6.4.0.0^{2,6}]dodeca-1(8),2(6),9-trien-10-yl)propanoic acid) present in the crystal structure was included in modeling. The global quality score assessed by SWISS-MODEL was 0.68 (QMEANDisCo) and model quality using Molprobity[45] indicated a score of 2.08, a clash score of 2.02, and 4.08% outliers in the Ramachandran plot. The model was downloaded and aligned with the $ExoT_{ART}$:14-3-3b structure in Chimera 1.16.[46] The $ExoT_{ART}$ molecules were removed to show only the $AexT_{ART}$ model sitting on top of the 14-3-3β dimer. To illustrate the active site, the model was aligned with the structure of an $ExoS_{ART}$:14-3-3β complex (PDB: 6GNK) co-crystallized with a carba-NAD molecule.[18] The $ExoS_{ART}$:14-3-3β complex was removed to show only the carba-NAD molecule in the active site of $AexT_{ART}$. The AlphaFold[47] prediction of $AexT_{FL}$ was downloaded from Uniprot and the ART domain was superimposed with the SWISS-MODEL in Chimera 1.16.

Molecular cloning

Codon-optimized cDNAs of the ART domains ($AexT_{ART}$, residues 252-475 and $ExoT_{ART}$ residues 235-457) for expression in *Escherichia coli* strains were obtained from GeneArt (ThermoFisher). 6xHis-$ExoT_{ART}$:14-3-3β and 6xHis-$AexT_{ART}$:14-3-3β pET-Duet-1 co-expression vectors were previously constructed in the host laboratory (14-3-3β cDNA YWHAB).
The cDNA encoding the full-length exotoxins was propagated by PCR from whole-cell lysates of *Aeromonas salmonicida* strain A449 and *Pseudomonas aeruginosa* strain PAK and cloned as N-terminal hexahistidine fusions into pNIC28-Bsa4 vectors (Protein Science Facility, Karolinska Institutet).

The above-mentioned plasmids were used to sub-clone the full-length toxins from pNIC28-Bsa4 into the pET-Duet-1 expression vector to enable co-expression of 14-3-3β and exotoxin from two independent T7 promotors. Plasmids were digested with restriction enzymes XbaI (NEB, R0145S) and HindIII (NEB, R0104S) for 1h at 37°C. The backbone vector (pET-Duet-1, containing 14-3-3β in MCS1) and inserts (full-length toxins) were extracted from an agarose gel and ligated with Quick Ligase (NEB, M2200S) for 5 min at ambient temperature. The ligation was directly transformed into NEB5α competent cells (NEB, C2987). Positive clones were identified

via restriction digest and gel electrophoresis and sequences were confirmed by Sanger sequencing.

Protein expression tests in *E.coli*

Expression plasmids were transformed into a range of commercially available or homemade expression cell lines (generally T7 express (NEB c2566H) or BL21(DE3)T1R (homemade; carrying the pRARE2 plasmid (Karolinska Institutet Protein Science Facility)); other cell lines used were BL21(DE3) (NEB c2527H) and LEMO21(DE3) (NEB c2528)). Multiple colonies were inoculated in 11-15 ml Terrific Broth media (SigmaAldrich) supplemented with appropriate antibiotics (100 µg ml^{-1} Ampicillin, 50 µg ml^{-1} Kanamycin, 34 µg ml^{-1} Chloramphenicol). The cells were grown at 37°C at 200 rpm until they reached the desired density (generally OD600 ~0,7). The cell culture medium was cooled down to 18°C before overnight induction at 200 rpm. In cases where I was merely interested in the general expression and not protein solubility (as in **Fig. 1A, B**) induction was performed at 37°C for 3h at 200 rpm. Induction was started by the addition of 0.5 mM Isopropyl-β-D-thiogalactopyranosid (IPTG) unless indicated otherwise.

For the analysis of the effect of different additives in the culture medium, I set up 150 ml culture which I split into 12,5 ml aliquots after the desired density was reached. The cultures were then treated with 0.5 M NaCl, 5 mM betaine hydrochloride, 5 mM L-glutamic acid, or 10 mM benzyl alcohol as indicated in **figure 1C**. The cells were allowed to recover from the addition of the chemicals for 30 min while cooling down to 18°C before IPTG was added. Induction was performed overnight at 200 rpm. Inducer was removed by centrifugation at 2000 x g and resuspension in fresh Terrific Broth media supplemented with antibiotics. The cell culture was incubated for another 2h at 18°C.

Cells were pelleted at 4400 x g, 4°C and lysed in 3 ml lysis buffer (50 mM HEPES pH 7.5, 500 mM NaCl, 10% glycerol, 1 mM TCEP) supplemented with 10% B-Per (ThermoScientific), protease inhibitor cocktail (SIGMAFAST, S8830-20TAB) and DNAse I (1:100) per gram wet weight cells. Cells were lysed with freeze-thaw cycles and insoluble material was pelleted via centrifugation at 20,000 x g, 4°C for 15 min. Parts of the pellets were resuspended in lysis buffer and subjected to SDS-Page analysis together with the soluble fraction (NuPage 4-12% Bis-Tris gels; Invitrogen). The gels were stained with Coomassie.[48]

Protein expression and purification from the soluble fraction

Constructs were expressed in homemade pRARE2 (BL21(DE3)T1R cells (SigmaAldrich) carrying the pRARE2 plasmid (Karolinska Institutet Protein Science Facility)) or commercial BL21 (NEB, C2530H) competent cells. Cultures were set up in 2 L Schott glass bottles containing 1.5 L Terrific Broth media (SigmaAldrich) supplemented with 100 µg $µl^{-1}$ Ampicillin. Cells were grown at 37°C in a LEX Bioreactor (Epiphyte3) until OD_{600} reached 2. The temperature was reduced to 19°C and

protein overexpression was induced with 0.5 mM IPTG for 16 h. Cells were pelleted by centrifugation at 4400 x g, 4°C, and resuspended in 2.5 ml lysis buffer (50 mM HEPES pH 7.5, 500 mM NaCl, 10% glycerol, 1 mM TCEP supplemented with one tablet protease inhibitor cocktail (SIGMAFAST, S8830-20TAB) and 5 µl benzonase (SigmaAldrich)) per gram of wet weight cells. The suspension was sonicated on ice for 4 min in 10 s intervals and subsequently centrifuged at 22,000 x g for 25 min, 4°C. The supernatant was clarified using a 0.45 µm syringe filter before loading onto a 5 ml HiTrap TALON column (Cytiva, 28-9537-67). The bound protein was eluted with 50 mM HEPES pH 7.5, 500 mM NaCl, 300 mM imidazole, 10% glycerol, and 1 mM TCEP over a 5-column volume gradient. Peak fractions were analyzed by gel electrophoresis (NuPage 4-12% Bis-Tris gels; Invitrogen) and Coomassie staining[48] before subsequent purification steps.

For cation exchange chromatography of $AexT_{ART}$:14-3-3β, pooled IMAC fractions from the previous step were first desalted using a HiPrep 26/10 desalting column (Cytiva, 17-5087-01). The column was equilibrated in binding buffer (20 mM MES pH 6.0, 1 mM $MgCl_2$, 1 mM TCEP) and the elution was monitored on an ÄKTA system. Salt-free fractions were pooled together. If precipitation was observed, samples were centrifuged and filtered through a 0.45 µm syringe filter before subjecting them to a 5 ml HiTrap Heparin HP column (Cytiva, 17040701) equilibrated in binding buffer. Elution was performed over a 10-column volume gradient in elution buffer (20 mM MES, 1 mM $MgCl_2$, 1 M NaCl, 1 mM TCEP). The peak fractions were analyzed on a NuPage 4-12% Bis-Tris gel (Invitrogen) and further purified by gel filtration.

For size exclusion chromatography protein samples were loaded on a HiLoad 16/600 Superdex 75 pg column (Cytiva, 28-9893-33) equilibrated in 50 mM Hepes pH 7.5, 500 mM NaCl, 10% glycerol, 1 mM TCEP (glycerol was omitted for purifications intended for mass spectrometry). Protein purity was checked on a NuPage 4-12% Bis-Tris gel (Invitrogen). Pure fractions were pooled and concentrated with Vivaspin centrifugal concentrators (SigmaAldrich, Z614025 or similar). Samples were frozen in aliquots and stored at -80°C.

Protein purification from the insoluble fraction – Recovery from inclusion bodies

Protein overexpression was performed as described above. Cells were pelleted at 4400 x g, 4°C. The cell pellet was homogenized at room temperature in 4 ml lysis buffer per gram wet weight of cells using a glass-glass homogenizer (lysis buffer: 50 mM Tris pH 7.5, 500 mM NaCl, 10% glycerol, 1.5 mM EDTA, 0.5 mM TCEP supplemented with 20% B-PER, Benzonase (8 µl L^{-1} cell culture; SigmaAldrich) and 200 µg ml^{-1} lysozyme). The lysate was sonicated three times on ice for 4 min, in 10 s intervals, and then centrifuged for 25 min at 22,000 x g, 4°C. The insoluble fraction containing the inclusion bodies was collected and the supernatant discarded.

The pellet was resuspended in 5 ml wash buffer A per gram of wet weight cells (100 mM Tris pH 7.5, 500 mM NaCl, 2 M Urea, 10 mM EDTA, 5 mM TCEP, 2% Triton X-100) with the help of a

glass-glass homogenizer. The suspension was centrifuged at 15,000 x g, 15 min, and 4°C to pellet inclusion bodies. This washing step was performed three times. Then the pellet was resuspended in 5 ml wash buffer B per gram of wet weight cells (100 mM Tris pH 7.5, 10 mM EDTA). The suspension was centrifuged at 15,000 x g, 10 min, 4°C, and the supernatant was discarded. The pellet was resuspended in 1 ml solubilization buffer (6.6 M GndHCl, 50 mM Tris pH 8) per 20-40 mg inclusion bodies, using a manual glass-glass homogenizer. The suspension was incubated for 2-3 h at room temperature and under constant stirring. Cell debris and non-solubilized material were removed by centrifugation at 50,000 x g for 20 min.

The protein-containing supernatant was either subjected directly to dialysis (see below) or incubated with Ni-NTA agarose beads (Qiagen) at room temperature overnight under gentle shaking. The beads were spun down and washed two times with 6 M GdnHCl, 50 mM Tris pH 8. An additional wash step with 6 M GdnHCl, 50 mM Tris pH 8.0, and 12 mM imidazole was performed to remove contaminants. The protein of interest was eluted in 6 M GdnHCl, 50 mM Tris pH 8.0, and 400 mM imidazole. As guanidine precipitates in the presence of SDS, ethanol precipitation was required for SDS-page analysis. Ice-cold 98% ethanol was added in 9-fold excess to aliquots of the eluates. The samples were vortexed and incubated at -80°C for 20 min. The precipitate was pelleted by centrifugation at 20,000 x g for 15 min, 4°C. The supernatant was removed and the pellet was resuspended in deionized water. This suspension was then used for gel electrophoresis.

The protein concentration of the solubilized protein solution was determined on a Nanodrop Lite spectrophotometer (ThermoScientific). Before refolding, the Ni-NTA beads eluate was diluted to a final concentration of 0.1 mg/ml with 6 M GndHCl, 50 mM Tris pH 8.0. If the Ni-NTA beads step was omitted, the protein concentration was kept at 2 mg/ml. Step-wise dialysis was performed at room temperature under gentle stirring, using 14,000 kDa cut-off high retention, seamless cellulose tubings (Sigma, D0405-100FT). Each dialysis step was performed in approximately 80 ml buffer per ml of protein solution for at least 2h, using the following buffers with decreasing GndHCL concentration: Buffer A (4 M GndHCl, 50 mM Tris pH 7.5), buffer B (2 M GndHCl, 50 mM Tris pH 7.5), buffer C (0.5 M GndHCl, 50 mM Tris pH 7.5), buffer D (50 mM Tris pH 7.5, 300 mM NaCl, 10% glycerol, 0.5 mM TCEP). Before starting the final dialysis step, human 14-3-3β was added in approximately equimolar concentrations to the toxins to assist in proper refolding. The refolded proteins were centrifuged for 5 min, 4000 x g to remove possible aggregates and concentrated with Vivaspin 20 centrifugal concentrators (30 kDa MWCO, SigmaAldrich, GE28-9323-61). The samples were frozen in aliquots and the success of refolding was evaluated in an εNAD^+ assay.

Dynamic light scattering

Protein complexes were analyzed using a Zetasizer μV instrument (Malvern Panalytical). Protein batches were thawed, centrifuged at 17,000 x g for 20 min and diluted in filtered solvent (50 mM HEPES pH 7.5, 300 mM NaCl, 10% glycerol, 0.5 mM TCEP) to a concentration that gave count rates between 100 and 300 kcps ($ExoT_{ART}$: 0.36 mg/ml, $AexT_{ART}$: 0.3 mg/ml and $AexT_{FL}$: 0.34 mg/ml). The samples (final volume 100 μl) were measured in polystyrene cuvettes (ZEN0118, Malvern Panalytical) using the default protein SOP method of the Zetasizer Software. Measurement was performed at 20°C with an equilibration time of 60 s. Each measurement was performed in triplicates. The results were exported and re-plotted in Prism (GraphPad Software).

Size Exclusion Chromatography – Multi-Angle Light Scattering (SEC-MALS)

The oligomeric state of the exotoxin:14-3-3β complexes was analyzed at LP3 (Lund University Protein Production Platform) using the OMNISEC system (Malvern Panalytical). Prepared protein aliquots were thawed on ice and filtered with 0.2 μm centrifugal filters (Millipore). The samples were kept at 4°C until they were injected into the system equilibrated in 50 mM HEPES pH 7.5, 300 mM NaCl and 1 mM TCEP. The system is composed of the OMNISEC RESOLVE module (integrating a Superdex 200 Increase 10/300 GL (Cytiva), with a combined pump, degasser, autosampler, and column oven) and the OMNISEC REVEAL, an integrated multi-detector module measuring light scattering (RALS 90° angle and LALS 7° angle), differential refractive index, viscosity and UV/VIS absorption. The detectors were normalized with bovine serum albumin (ThermoFisher). Each sample was injected in duplicates of 120 μl each, corresponding to 68 μg ($ExoT_{ART}$), 55 μg ($AexT_{ART}$), and 58 μg ($AexT_{FL}$) protein per injection. The system was run at 0.5 ml/min. Data was collected and analyzed with the OMNISEC v11.32 integrated software provided by Malvern. A representative run was chosen for analysis. The refractive index and measured molecular weight parameters as a function of retention volume were re-plotted in Prism (GraphPad Software).

Enzyme kinetics – εNAD$^+$ assay

ADP-ribosylation activity of the toxins was assayed in an εNAD$^+$ assay. The hydrolysis of the NAD$^+$ analog 1,N^6-etheno-NAD$^+$ (εNAD$^+$) into nicotinamide and εADP-ribose can be followed by a 10-fold increase in the fluorescence intensity. εAMP possesses the same extinction coefficient as εADP-ribose and can therefore be used for calibration.[34] An εAMP calibration curve was generated, titrating εAMP (Jena Bioscience) in reaction buffer (0, 1, 2, 4, 8. 16, 32, 64 μM εAMP) in a final volume of 50 μl. Focus and gain adjustment was performed based on the highest εAMP concentration (maximum gain adjustment set to 90%). The εAMP fluorescence was measured in top-optic endpoint mode with a 302-20 nm excitation filter and a 410-20 nm emission filter in a CLARIOstar multimode plate reader (BMG Labtech). The same electronic enhancement and optic settings were then used for the entire measurement. 50 μl reactions containing 200 nM exotoxin

and 400 nM 14-3-3-β were prepared in 20 mM HEPES pH 7.5, 50 mM NaCl, 4 mM $MgCl_2$, 0.5 mM TCEP. In reactions with agmatine (SigmaAldrich), εNAD$^+$ concentration was kept at 25 µM. Reactions were started by the addition of εNAD$^+$ (Roche) and pipetted into black 96-well half-area non-binding plates (Corning, CLS3993). Every reaction was set up as a technical triplicate. Fluorescence intensity increase was followed over a 30-min time course. The linear range was analyzed and the data was plotted in Prism (GraphPad Software). The εAMP calibration curve was used to convert fluorescence increase per time to processed εNAD$^+$ (in µM) per time. The slopes (i.e. processing rates in µM min^{-1}) were determined by linear regression analysis and plotted as a function of substrate concentration (εNAD$^+$ or agmatine). To determine the specific ADP-ribosyltransferase activity over agmatine, the processing rates obtained without agmatine were subtracted. Michaelis-Menten least-squares fit analysis was performed to obtain kinetic constants (V_{max} and K_m). The catalytic constant (k_{cat}) gives an estimate of how many substrate molecules one single enzyme can process into a product molecule per unit time and is determined as

$$k_{cat} = \frac{V_{max}}{[E]_0}$$

where V_{max} is the maximum velocity of the reaction and
$[E]_0$ is the enzyme concentration.

The efficiency of an enzyme over a specific substrate is given by

$$\text{catalytic efficiency} = \frac{k_{cat}}{K_m}$$

where k_{cat} is the catalytic constant and
K_m is the substrate concentration at half-maximum velocity and is often used to infer the affinity of the enzyme for the substrate.

For a good substrate, a high k_{cat} and a low K_m are expected, resulting in a high catalytic efficiency.

Preparation of cell lysates for protein overlay assays

Approximately 10x10^6 Jurkat cells (E6-1; modified to express the adhesion molecule rCD48 and MHC class II HLA-DQ8) were washed in 1 ml ice-cold D-PBS and lysed in 200 µl hypotonic buffer (50 mM Tris pH 7.5, supplemented with protease (Complete, Roche, 11504400) and phosphatase (PhosSTOP EASYpack, Roche, 04906845001) inhibitor cocktails). The cells were resuspended by pipetting thoroughly during 15 min incubation on ice. Protein concentration was determined on a nanodrop and 0.1% benzonase (SigmaAldrich) was added. The lysate was aliquoted and temporarily stored at -80°C.

Analysis of toxin target spectrum - Protein overlay assays

ADP-ribosylation reactions for the analysis of target substrates on protein overlay assays were performed with 100 µM NAD-mix, containing 10% spiked-in biotin-NAD^+ (BPS-80610, Nordic BioSite) in NAD^+ (Roche). Enzyme concentrations were kept at 1 µM 14-3-3-dependent toxins, 2 µM PARP10 catalytic domain, and 20 nM *Clostridium botulinum* C2I toxin subunit, unless indicated otherwise. Final reactions with ExoT and AexT contained 2x excess 14-3-3β (either from co-expression or chaperone-assisted refolding plus additionally added) and 10 µM substrate. For reactions with Jurkat cell lysate, I added 10 µg total protein per 20 µl reaction. 20-40 µl reactions were set up in 0.2 ml microtubes in reaction buffer (20 mM HEPES 7.5, 50 mM NaCl, 4 mM $MgCl_2$, 0.5 mM TCEP) and the reactions were started by the addition of NAD-mix, or toxin. The reactions were incubated for 1 h at ambient temperature and stopped by the addition of Laemmli buffer and boiling at 95°C for 4 min. Proteins were separated on a 4-12% Bis-Tris polyacrylamide gel (Invitrogen) at 200 V for 40 min and subsequently transferred onto a PVDF membrane in transfer buffer (3% (m/v) trizma, 14.4% (m/v) glycine and 10% (v/v) methanol) for 1h at 160 mA. Ponceau S staining of the membrane served as a control for loaded protein and transfer efficiency. The membranes were de-stained, blocked for 1h in 1% BSA in TBS-T buffer, and incubated for 1h in 0.5 µg/ml HRP-linked Streptavidin (21126, ThermoScientific) in 1% BSA in TBS-T buffer. Proteins modified with Biotin-ADP-ribosylations were visualized with SuperSignal™ West Pico PLUS Chemiluminescent Substrate (ThermoScientific). Images were obtained in a Syngene PXi imaging system.

Quantification of the removal of auto-ADP-ribosylation by specific ADP-ribosylhydrolases - MacroGreen method

Auto-ADP-ribosylation reactions at 250 nM exotoxin and 500 nM 14-3-3β were carried out in reaction buffer (25 mM HEPES pH 7.5, 100 mM NaCl, 0.2 mM TCEP, 4 mM $MgCl_2$) in the presence of 1 mM NAD^+ at ambient temperature for 30 min, under constant shaking at 150 rpm. As a control, NAD^+ was omitted. The reactions were then transferred into a 96-well high-binding plate (Nunc MaxiSorp™), creating eight replicates of 50 µl each. Eight additional wells were filled with 50 µl reaction buffer that were later used to determine the background signal. The proteins were allowed to bind to the plate for 30 min at room temperature and shaking at 250 rpm. The wells were rinsed 3x with 150 µl reaction buffer to remove excess NAD^+ before blocking with 1% BSA in reaction buffer for 5 min (150 µl/well). The wells were rinsed 2x with 150 µl reaction buffer, then 50 µl of ADP-ribosylhydrolase reactions (ARH1, MacroD2, or ARH3 at 1.5 µM) in reaction buffer were added per well. Wells without ADP-ribosylhydrolases were filled with 50 µl reaction buffer instead. The reactions were allowed to proceed for 1h at 250 rpm. The wells were rinsed 2x with 150 µl reaction buffer and were then filled with 100 µl 1 mM ADP-ribose in reaction buffer. After 10 min, ADP-ribose was removed and the wells were rinsed 3x with 150 µl Tris-buffered

saline with 0.1% Tween20 (TBS-T buffer). Another 5 min blocking step with 1% BSA in TBS-T buffer was performed (150 µl/well). The wells were rinsed 2x with 150 µl TBS-T buffer. The ADP-ribosylation was detected with the GFP-fused macrodomain of *Archaeoglobus fulgidus* (eAF1521) that carries mutations that yield higher affinity for ADP-ribose (described in detail in García-Saura et al. 2021).[39] 1 µM of eAF1521-GFP in 50 µl TBS-T buffer was added per well followed by incubated for 5 min. Unbound eAF1521-GFP was removed by three washes with 150 µl TBS-T buffer. 150 µl TBS-T buffer was added per well for readout. GFP fluorescence was measured on a CLARIOstar multimode reader (BMG Labtech) in top-optic, endpoint mode with an excitation filter of 470-15 nm and an emission filter of 515-20 nm. The data was normalized to the background signal (blank wells) and the % remaining ADP-ribose was determined according to the auto-modification reaction (no ADP-ribosylhydrolases added). The normalized data was plotted in Prism (GraphPad Software) and the significance was determined with a Welch ANOVA test, in which the mean of each column was compared to the mean of the auto-modification reaction.

Actin polymerization assay

Cytosolic β-actin from *Bos taurus*[49] in G-actin buffer (20 mM HEPES pH 7.5, 0.2 mM $CaCl_2$, 0.2 mM ATP, 0.5 mM TCEP) was thawed and diluted 1:1 in fresh G-actin buffer. The thawed and diluted sample was centrifuged for 15 min at max. speed, 4°C, and the supernatant was transferred to a new tube. 200 µM NAD^+, 10 µM β-actin, 400 nM exotoxin (ExoT and AexT variants), and 400 nM 14-3-3β or 20 nM *Clostridium botulinum* C2I toxin subunit in G-actin buffer were incubated in 100 µl reactions for 30 min at ambient temperature. Actin polymerization was subsequently triggered by the addition of 100 mM KCl and 2 mM $MgCl_2$. The reactions were transferred into airfuge tubes (Beckman Coulter, 342630) and allowed to proceed for 45 min at ambient temperature. Actin polymers were sedimented by ultracentrifugation in a Beckman Airfuge (A-100/18 rotor) for 15 min at 30 psi (corresponding to roughly 149,000 x g). The supernatant was separated from the pellet and the pellet resolved in an equal volume of G-actin buffer. Equal volumes of supernatant and pellet fractions were loaded on a 4-12% NuPage Bis-Tris gel (Invitrogen) and subjected to gel electrophoresis. The gel was stained with Coomassie.[48]

REFERENCES

1. L., A., Zhang, D., Souza, R. F. de, Anand, S. & Iyer, L. M. The Natural History of ADP-Ribosyltransferases and the ADP- Ribosylation System. *Curr Top Microbiol Immunol* **384**, 3–32 (2015).

2. Cohen, M. S. & Chang, P. Insights into the biogenesis, function, and regulation of ADP-ribosylation. *Nat. Chem. Biol.* **14**, 236–243 (2018).

3. Sung, V. M. H. Mechanistic overview of ADP-ribosylation reactions. *Biochimie* **113**, 35–46 (2015).

4. Deng, Q. & Barbieri, J. T. Molecular mechanisms of the cytotoxicity of ADP-ribosylating toxins. *Annu. Rev. Microbiol.* **62**, 271–288 (2008).

5. Simon, N. C., Aktories, K. & Barbieri, J. T. Novel bacterial ADP-ribosylating toxins: Structure and function. *Nat. Rev. Microbiol.* **12**, 599–611 (2014).

6. Gellatly, S. L. & Hancock, R. E. W. Pseudomonas aeruginosa: New insights into pathogenesis and host defenses. *Pathog. Dis.* **67**, 159–173 (2013).

7. Aktories, K., Lang, A. E., Schwan, C. & Mannherz, H. G. Actin as target for modification by bacterial protein toxins. *FEBS J.* **278**, 4526–4543 (2011).

8. Popoff, M. R. Bacterial factors exploit eukaryotic Rho GTPase signaling cascades to promote invasion and proliferation within their host. *Small GTPases* **5**, (2014).

9. Sun, J. & Barbieri, J. T. Pseudomonas aeruginosa ExoT ADP-ribosylates CT10 regulator of kinase (Crk) proteins. *J. Biol. Chem.* **278**, 32794–32800 (2003).

10. Vallis, A. J., Finck-Barbançon, V., Yahr, T. L. & Frank, D. W. Biological effects of Pseudomonas aeruginosa type III-secreted proteins on CHO cells. *Infect. Immun.* **67**, 2040–2044 (1999).

11. Fehr, D. *et al.* Aeromonas exoenzyme T of Aeromonas salmonicida is a bifunctional protein that targets the host cytoskeleton. *J. Biol. Chem.* **282**, 28843–28852 (2007).

12. Vanden Bergh, P. & Frey, J. Aeromonas salmonicida subsp. salmonicida in the light of its type-three secretion system. *Microb. Biotechnol.* **7**, 381–400 (2013).

13. Menanteau-Ledouble, S., Kumar, G., Saleh, M. & El-Matbouli, M. Aeromonas salmonicida: Updates on an old acquaintance. *Dis. Aquat. Organ.* **120**, 49–68 (2016).

14. Janda, J. M. & Abbott, S. L. The genus Aeromonas: Taxonomy, pathogenicity, and infection. *Clin. Microbiol. Rev.* **23**, 35–73 (2010).

15. Garrity-Ryan, L. *et al.* The arginine finger domain of ExoT contributes to actin cytoskeleton disruption and inhibition of internalization of Pseudomonas aeruginosa by epithelial cells and macrophages. *Infect. Immun.* **68**, 7100–7113 (2000).

16. Barbieri, J. T. & Sun, J. Pseudomonas aeruginosa ExoS and ExoT. *Rev. Physiol. Biochem. Pharmacol.* **152**, 79–92 (2004).

17. Coburn, J., Kane, A. V., Feig, L. & Gill, D. M. Pseudomonas aeruginosa exoenzyme S requires a eukaryotic protein for ADP-ribosyltransferase activity. *J. Biol. Chem.* **266**, 6438–6446 (1991).

18. Karlberg, T. *et al.* 14-3-3 proteins activate Pseudomonas exotoxins-S and -T by chaperoning a hydrophobic surface. *Nat. Commun.* **9**, (2018).

19. Stevers, L. M. *et al.* Modulators of 14-3-3 Protein-Protein Interactions. *J. Med. Chem.* **61**, 3755–3778 (2018).

20. Krall, R., Schmidt, G., Aktories, K. & Barbieri, J. T. Pseudomonas aeruginosa ExoT is a Rho GTPase-activating protein. *Infect. Immun.* **68**, 6066–6068 (2000).

21. Kazmierczak, B. I. & Engel, J. N. Pseudomonas aeruginosa ExoT acts in vivo as a GTPase-activating protein for RhoA, Rac1, and Cdc42. *Infect. Immun.* **70**, 2198–2205 (2002).

22. Garrity-Ryan, L. *et al.* The ADP Ribosyltransferase Domain of Pseudomonas aeruginosa ExoT Contributes to Its Biological Activities. *Infect. Immun.* **72**, 546–558 (2004).

23. Braun, M. *et al.* Characterization of an ADP-ribosyltransferase toxin (AexT) from Aeromonas salmonicida subsp. salmonicida. *J. Bacteriol.* **184**, 1851–1858 (2002).

24. Kumar, R. *et al.* Evolutionary features in the structure and function of bacterial toxins. *Toxins (Basel).* **11**, (2019).

25. Han, S. & Tainer, J. A. The ARTT motif and a unified structural understanding of substrate recognition in ADP-ribosylating bacterial toxins and eukaryotic ADP-ribosyltransferases. *Int. J. Med. Microbiol.* **291**, 523–529 (2001).

26. Sun, J., Maresso, A. W., Kim, J. J. P. & Barbieri, J. T. How bacterial ADP-ribosylating toxins recognize substrates. *Nat. Struct. Mol. Biol.* **11**, 868–876 (2004).

27. Ménétrey, J. *et al.* NAD binding induces conformational changes in Rho ADP-ribosylating Clostridium botulinum C3 exoenzyme. *J. Biol. Chem.* **277**, 30950–30957 (2002).

28. Waterhouse, A. *et al.* SWISS-MODEL: Homology modelling of protein structures and complexes. *Nucleic Acids Res.* **46**, W296–W303 (2018).

29. Holbourn, K. P., Shone, C. C. & Acharya, K. R. A family of killer toxins: Exploring the mechanism of ADP-ribosylating toxins. *FEBS J.* **273**, 4579–4593 (2006).

30. de Marco, A., Vigh, L., Diamant, S. & Goloubinoff, P. Native folding of aggregation-prone recombinant proteins in Escherichia coli by osmolytes, plasmid- or benzyl alcohol-overexpressed molecular chaperones. *Cell Stress Chaperones* **10**, 329–339 (2005).

31. Cabrita, L. D. & Bottomley, S. P. Protein Expression and Refolding – a practical guide to getting the most out of inclusion bodies. *Biotechnol. Annu. Riview* **10**, 31–50 (2004).

32. Yamaguchi, H. & Miyazaki, M. Refolding techniques for recovering biologically active recombinant proteins from inclusion bodies. *Biomolecules* **4**, 235–251 (2014).

33. Palmer, I. & Wingfield, P. T. Preparation and extraction of insoluble (Inclusion-body) proteins from Escherichia coli. *Curr. Protoc. Protein Sci.* **1**, 1–25 (2012).

34. Klebl, B. M. & Pette, D. A fluorometric assay for measurement of mono-ADP-ribosyltransferase activity. *Anal. Biochem.* **239**, 145–152 (1996).

35. Sluchanko, N. N. & Gusev, N. B. Oligomeric structure of 14-3-3 protein: What do we know about monomers? *FEBS Lett.* **586**, 4249–4256 (2012).

36. Barth, H., Hofmann, F., Olenik, C., Just, I. & Aktories, K. The N-Terminal Part of the Enzyme Component (C2I) of the Binary Clostridium botulinum C2 Toxin Interacts with the Binding Component C2II and Functions as a Carrier System for a Rho ADP-Ribosylating C3-Like Fusion Toxin. *Infect. Immun.* **66**, 1364–1369 (1998).

37. García-Saura, A. G. & Schüler, H. PARP10 multi-site auto-and histone marylation visualized by acid-urea gel electrophoresis. *Cells* **10**, 1–11 (2021).

38. Deng, Q., Sun, J. & Barbieri, J. T. Uncoupling Crk signal transduction by Pseudomonas exoenzyme

T. *J. Biol. Chem.* **280**, 35953–35960 (2005).

39. García-Saura, A. G., Herzog, L. K., Dantuma, N. P. & Schüler, H. MacroGreen, a simple tool for detection of ADP-ribosylated proteins. *Commun. Biol.* **4**, 1–8 (2021).

40. Rack, J. G. M. *et al.* (ADP-ribosyl)hydrolases: Structural Basis for Differential Substrate Recognition and Inhibition. *Cell Chem. Biol.* **25**, 1533-1546.e12 (2018).

41. Rosenthal, F. *et al.* Macrodomain-containing proteins are new mono-ADP-ribosylhydrolases. *Nat. Struct. Mol. Biol.* **20**, 502–507 (2013).

42. Fontana, P. *et al.* Serine ADP-ribosylation reversal by the hydrolase ARH3. *Elife* **6**, 1–20 (2017).

43. Riese, M. J. *et al.* Auto-ADP-ribosylation of Pseudomonas aeruginosa ExoS. *J. Biol. Chem.* **277**, 12082–12088 (2002).

44. Schüler, H., Nyåkern, M., Schutt, C. E., Lindberg, U. & Karlsson, R. Mutational analysis of arginine 177 in the nucleotide binding site of β-actin. *Eur. J. Biochem.* **267**, 4054–4062 (2000).

45. Williams, C. J. *et al.* MolProbity: More and better reference data for improved all-atom structure validation. *Protein Sci.* **27**, 293–315 (2018).

46. Pettersen, E. F. *et al.* UCSF Chimera - A visualization system for exploratory research and analysis. *J. Comput. Chem.* **25**, 1605–1612 (2004).

47. Jumper, J. *et al.* Highly accurate protein structure prediction with AlphaFold. *Nature* **596**, 583–589 (2021).

48. Yasumitsu, H., Ozeki, Y., Kawsar, S. M. A., Toda, T. & Kanaly, R. CGP stain: An inexpensive, odorless, rapid, sensitive, and in principle in vitro methylation-free Coomassie Brilliant Blue stain. *Anal. Biochem.* **406**, 86–88 (2010).

49. Schüler, H., Karlsson, R. & Lindberg, U. Purification of nonmuscle actin. in *Cell Biology: A laboratory handbook* (ed. Celis, J. E.) 165–171 (Elsevier Academic Press, 2006).

50. Goehring, U. M., Schmidt, G., Pederson, K. J., Aktories, K. & Barbieri, J. T. The N-terminal domain of Pseudomonas aeruginosa exoenzyme S is a GTPase- activating protein for Rho GTPases. *J. Biol. Chem.* **274**, 36369–36372 (1999).

APPENDIX

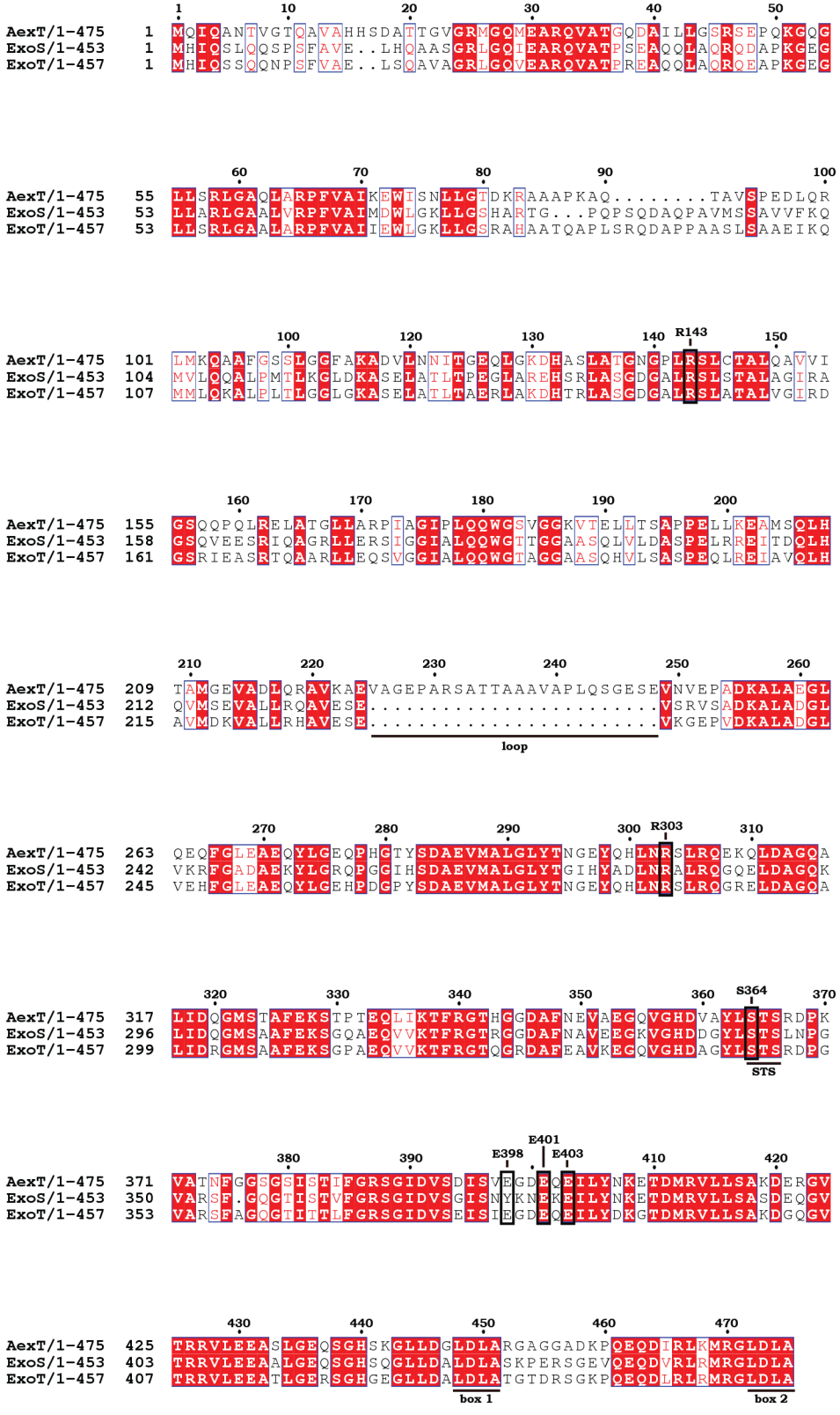

Figure legend on next page.

Appendix figure 1 Sequence alignment of full-length AexT, ExoS, and ExoT. Sequences were aligned with the ClustalO algorithm in Jalview. The final image was generated with Espript 3.0. The catalytic site residues are indicated with black boxes (AexT numbering). R143 is necessary for GAP activity.[11,21,50] E401 and E403 make up the canonical EXE motif that is present in other related RSE ARTs.[3,5,29] AexT replaces the E403 function with E398, resulting in an EXXE(XE) motif instead of an EXE motif.[11] Interestingly, ExoT also possesses an EXXEXE motif, although the catalytic residues reside within the EXE fraction.[9] R303 has also been shown to play a role in AexT catalysis[11] and is conserved with ExoT and ExoS. S364 is part of the conserved STS motif in RSE ARTs.[26,29] LDLA box 1 and box 2 as well as a disordered loop connecting the GAP and the ART domain that is absent in ExoT and ExoS are also indicated.

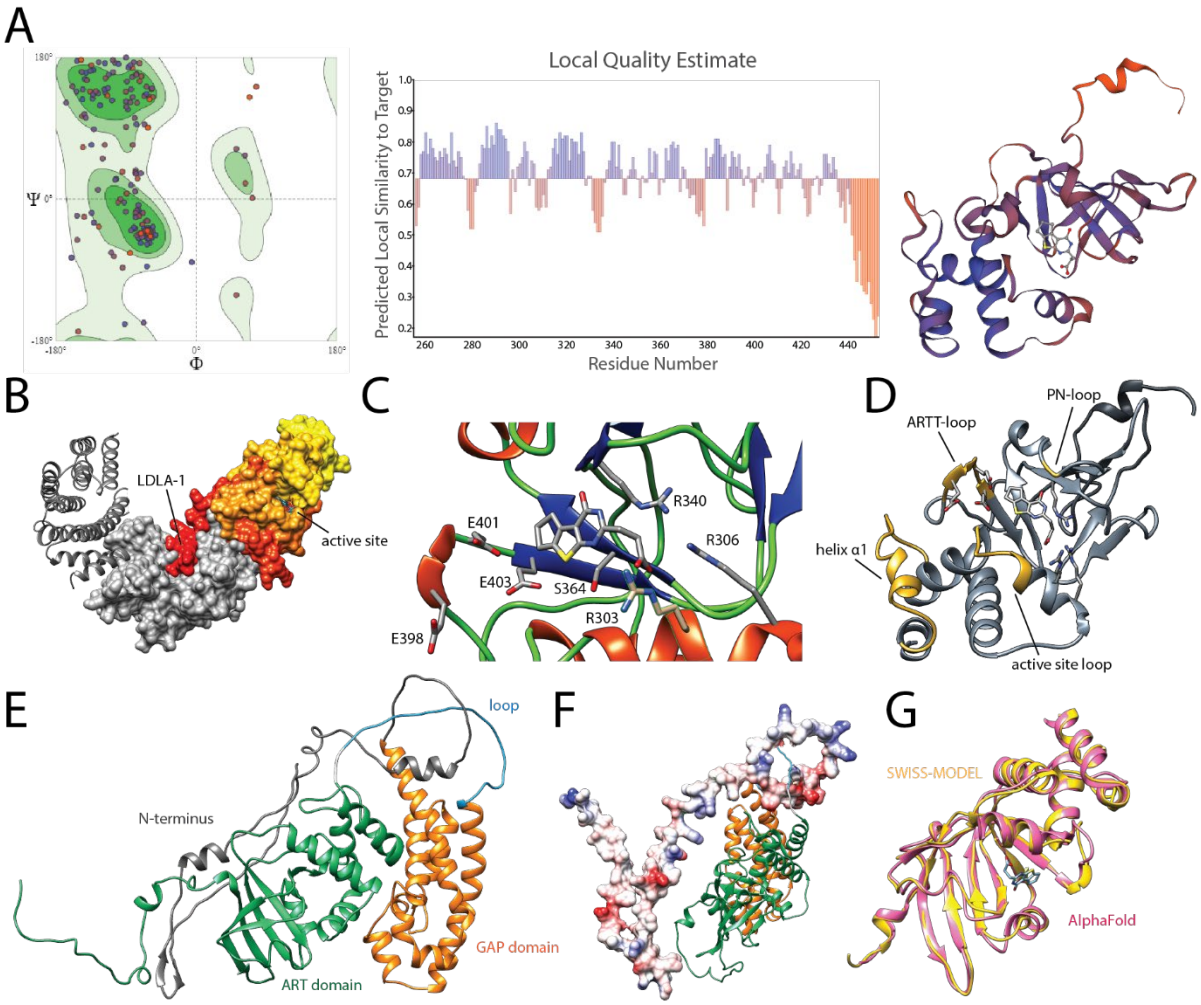

Appendix figure 2 Quality assessment and details of AexT$_{ART}$ homology model (A) Quality reports of the AexT$_{ART}$ SWISS-MODEL.[28] Left panel, Ramachandran plot with 4,08% outliers; central panel, per residue quality estimate with global quality score (QMEANDisCo) of 0.68 represented as the average of the local quality estimate; right panel, AexT$_{ART}$ model colored according to per residue quality estimate. Modeling of the unstructured C-terminus containing LDLA box 1 is less reliable. **(B)** LDLA-box 1 of the model fits well into the phosphoprotein binding site of 14-3-3β. **(C)** Close-up view of the active site shows arginine and glutamate residues in the proximity of the inhibitor STO1101, among which E398, E401, and R303 are essential for catalysis.[11] β-strands are in blue, α-helices in red, and loops in green. **(D)** Regions known to confer substrate specificity for CRK in ExoT[26] are labeled and highlighted in gold. **(E)** AlphaFold[47] model of AexT$_{FL}$. Individual domains are indicated; the loop colored in blue is absent in ExoT and ExoS. **(F)** The depiction of the electrostatic surface potential of the unstructured N-terminus in AexT$_{FL}$ containing a putative membrane localization domain illustrates its predominantly hydrophobic nature. **(G)** SWISS-MODEL in yellow superimposed with ART domain of the AlphaFold model in pink. RMSD across all 198 C$_α$ atom pairs: 1.403Å (0.772Å between 182 pruned atom pairs).

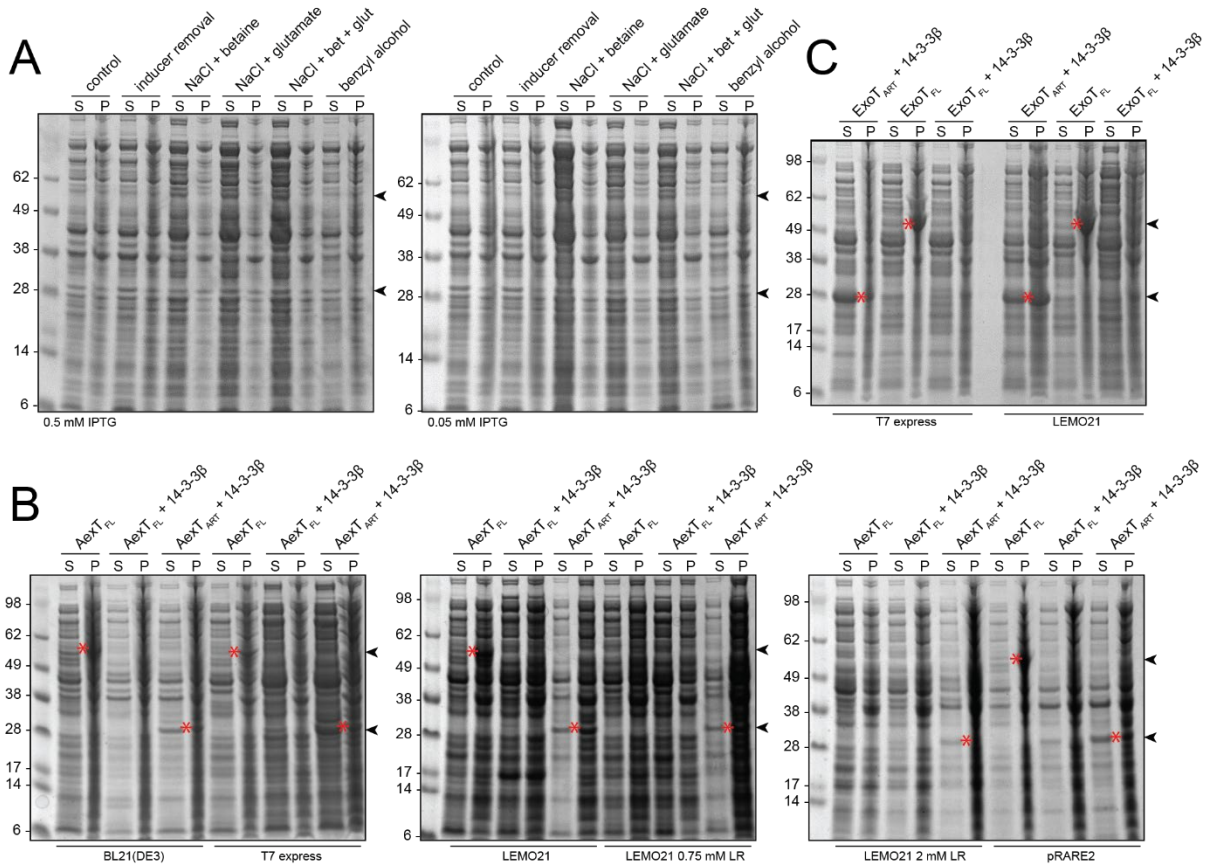

Appendix figure 3 Variation of expression conditions is ineffective to increase solubility of $ExoT_{FL}$ and $AexT_{FL}$. Arrowheads indicate the approximate theoretical molecular weight of constructs; asterisks indicate overexpression bands. **(A)** Variation of $AexT_{FL}$:14-3-3β expression conditions did not result in increased expression or shift to the soluble fraction. I tested different IPTG concentrations (here 0.5 and 0.05 mM IPTG), inducer removal after overnight induction, folding support by salt-induced accumulation of osmolytes (betaine and glutamate), or artificially induced heat shock response by the addition of benzyl alcohol.[30] **(B, C)** Expression tests of $AexT_{FL}$ **(B)** and $ExoT_{FL}$ **(C)** with different competent cells. Both, single- and co-expression with 14-3-3β were tested, alongside with ART domain 14-3-3β co-expression as a positive control. 14-3-3β is similar in size to the ART domains. LR, L-rhamnose. Details on experimental procedures are described in “Materials and Methods”.